Analysis of Human Motion Data for Vehicle Ingress Discomfort Evaluation

by

Hadi Ibrahim Masoud

A dissertation submitted in partial fulfillment
of the requirements for the degree of
Doctor of Engineering
(Manufacturing)
in The University of Michigan
2015

Doctoral Committee:

Professor Jionghua (Judy) Jin, Chair
Assistant Professor Eunshin Byon
Assistant Professor Clive D'Souza
Research Professor Matthew Reed

DEDICATION

This dissertation is dedicated to my wonderful parents for their endless love, support, and encouragement.

ACKNOWLEDGEMENTS

First, I would like to thank God; my guidance and success are fully attributed to him. I thank my loving parents for their continuous support and for always pushing me to do better. I thank the joys of my life, my kids, Hamza and Ammar, for their unconditional love. I thank my wife, Rana Mosli, who supported me in this journey that we took together.

I thank my advisor, Professor Judy Jin, for her guidance, support, and for believing that I can always do better. I thank Professor Matt Reed for always going out of his way to teach me something new. I also thank Professor Eunshin Byon and Professor Clive D'Souza for their valuable advice and support.

I would like to thank my sponsors, King Abdul-Aziz University and The University of Jeddah, for funding my education and enabling me to succeed. Further, I would like to thank Ford Motor Company for making these data available and Prof. Kerby Shedden, Director of the Center for Statistical Consultation and Research (CSCAR), for his time and invaluable statistical consultation.

Finally, I would like to thank all my friends for inspiring me and for supporting and carrying me during tough days. I specially want to thank my friend Hatim Bukhari for his kind heart and selfless support, and my friend Amr Alaa for always listening to my struggles.

TABLE OF CONTENTS

LIST OF TABLES

LIST OF FIGURES

Figure

ABSTRACT

The ease of entering a vehicle, known as ingress, is one of the important ergonomic factors that car manufacturers consider during the process of vehicle design. This has motivated vehicle manufacturers to focus on assessing and improving ingress discomfort. With the rapid advancement in human motion capture and computer simulation technologies, one of the promising means to evaluate vehicle ingress discomfort is through analyzing human motion data. For this purpose, this dissertation will focus on proposing methods that analyze human motion data to evaluate vehicle ingress discomfort.

The first part of this dissertation proposes a method for identifying and analyzing human motion variation patterns. The method uses a high-order array to represent human motion data and utilizes the Uncorrelated Multilinear Principal Component Analysis (UMPCA) method to identify variation patterns in human motion. The proposed method is capable of preserving the original spatiotemporal correlation structure of human motion data and provides better feature extraction than Principal Component Analysis (PCA). The method is applied to the ingress motion data to show its effectiveness in automatically detecting important motion variation patterns.

The second part of this dissertation proposes a method for modeling the relationship between ingress motion and ingress discomfort ratings. The method presents a modeling framework that predicts subjective responses using human motion trajectories. The

framework integrates curve alignment and data dimension reduction methods into the prediction model development. A case study is shown to demonstrate that human motion prediction models are more effective than simpler, more common ingress discomfort prediction models.

The third part of this dissertation proposes a method for statistical hypothesis testing and sample size calculation for comparing ingress discomfort proportions of different vehicle designs. A dual-bootstrap method is proposed to estimate the standard deviation of ingress discomfort proportions estimated using a human motion prediction model. The proposed method is capable of separating the two sources of variation; the modeling variance, which results from the uncertainty in the estimated prediction models, and the sampling variance, which arises due to the randomness in the prediction dataset. The effectiveness of the proposed method is demonstrated through an ingress case study.

The research presented in this dissertation is applicable beyond the analysis of ingress motion data; it can be applied to many fields where human motion data is available. At a broader level, the research presented can be useful in the analysis of functional data of many types, with particular applicability to multi-channel time-series data.

CHAPTER 1
Introduction

1.1 Motivation

The ease of getting into and out of a vehicle, known as ingress and egress, is one of the important factors used by J.D. Power for measuring customer satisfaction in the automotive industry (Morgans and Thorness 2013). Today, ingress/egress has become an essential ergonomic factor in vehicle design. This brings about a prominent research issue of how to effectively assess and predict customer ingress and egress discomfort during vehicle design.

Assessing ingress and egress discomfort is not an easy task. One of the popularly used methods is to build prototypes or mockups and use them to conduct *"participant tests."* These tests require recruiting a large number of participants to perform the ingress and egress motion and to provide discomfort ratings, which is an expensive and time-consuming process. With today's increasing pressure to reduce cost and time-to-market, manufacturers are constantly looking for cheaper and faster alternatives to evaluate vehicle ingress and egress discomfort. The rapid advancement of computer simulation technology has enabled virtual testing via computer simulation to evaluate a vehicle's ingress and egress discomfort. To develop such virtual tests, three research issues need to be studied: (1) how to build realistic human figure models; (2) how to simulate the motion of humans during ingress and egress; and (3) how to model the relationship between ingress and egress motion and participants' discomfort ratings.

As extensive research has been conducted in the fields of building human figure models (Badler *et al.* 2005) and simulating human motion during ingress (Reed *et al.* 2006, Reed and Huang 2008), this dissertation will focus on modeling the relationship between ingress motion and participants' ingress discomfort ratings. The developed methodology is also applicable for assessing egress discomfort.

Modeling the relationship between ingress motion and ingress discomfort ratings requires the use of human motion data from participant-tests. Once this model is built, it can then be used for virtual tests to assess and predict ingress discomfort ratings for simulated motions. To achieve this goal, the following three research issues will be addressed in this dissertation.

The first issue is how to systematically identify important ingress motion patterns that can reflect the variation among different participants. For example, one important motion pattern in the ingress motion might be the motion of the head and neck in the Z-direction as a participant enters the vehicle. This information can help designers better understand how changes in vehicle design affect human motion.

The second issue is how to develop a statistical model to understand the relationship between ingress motion and ingress discomfort ratings. This model is critically needed for predicting ingress discomfort ratings from simulated motion data.

The third issue is how to conduct a statistical analysis, such as statistical hypothesis testing and sample size calculation, for comparing the predicted ingress discomfort of different vehicle designs. Sample size calculation is of particular importance in cases relating to participant-tests, where the tests are costly and time-consuming. Therefore, the following three tasks will be conducted in this dissertation:

1. Analysis of human motion variation patterns using uncorrelated multilinear principal component analysis (UMPCA)
2. Predicting subjective responses using human motion for assessing vehicle ingress design
3. Sample size calculation for a functional human motion analysis

1.2 Background and Data Description

Ford Motor Co. performed a laboratory experiment to capture the motion of participants during the ingress and egress process. The 32 participants whose ingress and egress motions were captured span a wide range of the U.S. adult population from a 3rd percentile female stature to 98th percentile male stature. The participants also vary in weight and amount of body fat, ranging from very thin (BMI = 19) to obese (BMI = 52). Numerous anthropometric measurements were taken for each participant to ensure that a digital human manikin could be created to accurately represent the participants.

Ingress and egress motions were captured for 17 vehicle package configurations obtained by manipulating seven key design variables: seat height (H30), vehicle seat height above pavement (H5), vehicle roof height (H11), vertical distance between the ground and the vehicle floor (H130), lateral distance between the seating reference point (SgRP) and the outside edge of the vehicle (W18), lateral distance between SGRP and the roof rail (SgRP to Rail), and the fore-aft distance between the SgRP and the B Pillar (B-Pillar X). An illustration of these variables is shown in Figure 1-1. Moreover, the Cartesian coordinate system used for this analysis was based on the SAE J187 standard coordinate system used in vehicle engineering. A programmable vehicle buck, the Human Occupant Package Simulator (HOPS), was used to create the vehicle packages.

By choosing different levels of each design variable, different seat configurations can be made, for each of which participants will perform tests and provide their ratings on their ingress/egress discomfort ratings.

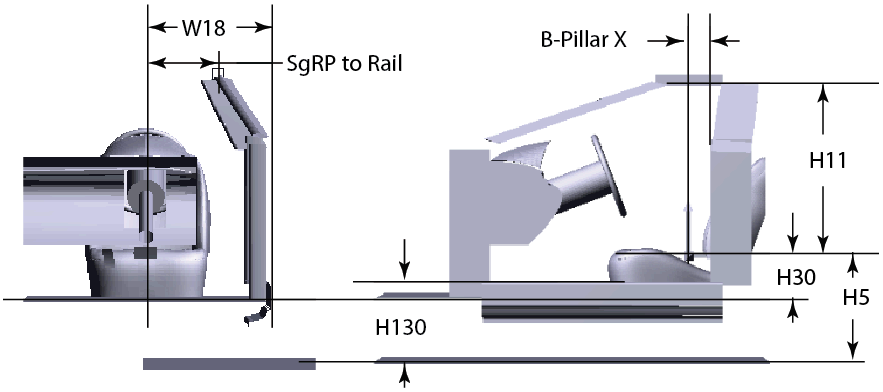

Figure 1-1. Car seat design variables

Vicon motion capture cameras were strategically located around the HOPS to avoid obstructions between the cameras and the body markers. A unique set of reflective markers was designed to capture whole-body motion. The markers were attached to both anthropometric landmarks as well as in clusters to some segments (such as the thigh) to ensure that joint motions could be reconstructed accurately.

Using custom software, the trajectories of markers place on the body were used to estimate the locations over time of 20 joints that define the kinematic linkage of the body. The 20 joints calculated are the right ankle, right knee, right toe, right shoulder, right elbow, right wrist, right clavicle, left hip, left ankle, left knee, left toe, left shoulder, left elbow, left wrist, left clavicle, head, neck, and the spinal vertebrae T12L1, T1T2, and S1L5. Figure 1-2 shows an example of the motion trajectories calculated from one ingress trial. Following the standard automotive industry convention, the trajectories were expressed in a coordinate system with the Z-axis vertical, X-axis oriented fore and aft along the vehicle longitudinal axis, and Y-axis “cross car”.

After participants completed an ingress/egress trial, they were asked to rate the trial. The participants were asked the following question: “Please rate the ease of getting in and out of this vehicle configuration.” The possible responses on a 10-point scale were 1–2 (unacceptable), 3–5 (average), 6–8 (outstanding), and 9–10 (truly exceptional). For the current analysis, these responses were transformed into 0/1 responses using a threshold (cutpoint), such as transforming a response to 1 if the rating was greater than 5.

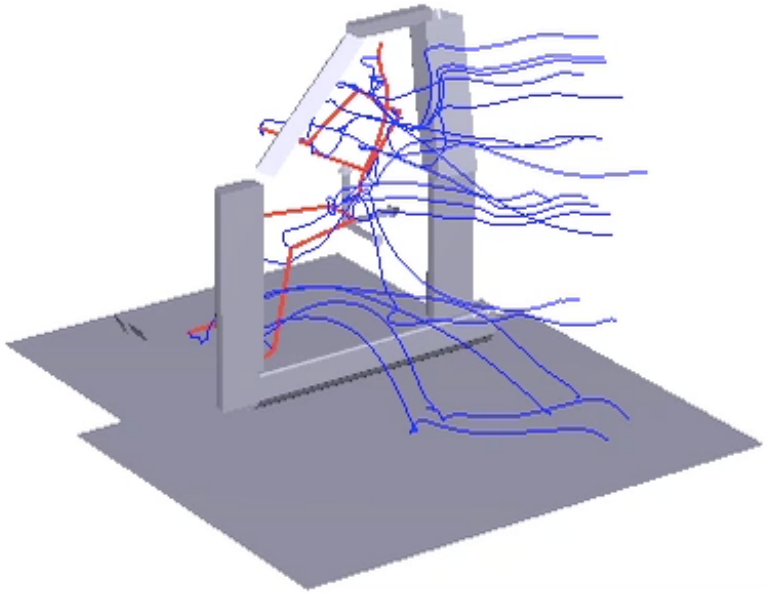

Figure 1-2. Ingress motion data of one participant

Figure 1-3 shows the distribution of the comfort rating for all vehicles. The ratings are roughly normally distributed with a slight right skew. Figure 1-4 shows the distribution of comfort ratings based on vehicle design. We can observe that some vehicles, such as vehicle design 1, has a consistent low comfort rating across all subjects, while vehicle designs, such as 3 and 5, have a wider range of response.

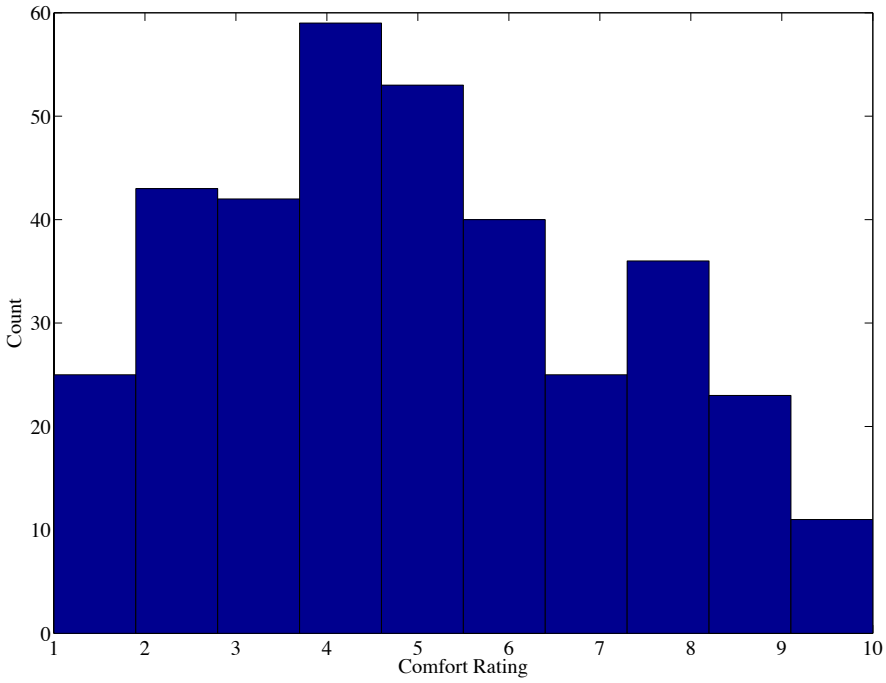

Figure 1-3. Distribution of comfort ratings

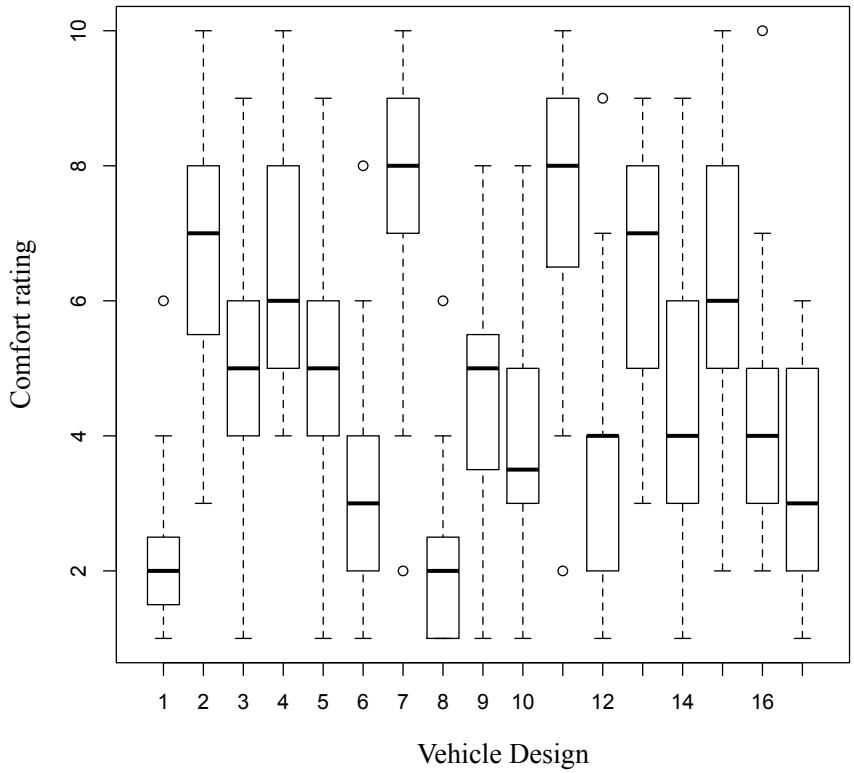

Figure 1-4. Comfort rating per vehicle design

1.3 Overview of Dissertation

The research topics outlined in Section 1.1 are discussed in this overview. For each topic, the research objectives, challenges, and the proposed methodology are summarized.

1.3.1 Analysis of Human Motion Variation Patterns Using UMPCA

The objective of this task is to develop a systematic method to automatically identify the important ingress motion patterns. The most significant challenge in achieving this objective is the high dimensionality and multistream structure of the ingress data described in Section 1.2.

One possible way of identifying motion patterns during ingress is through visual observation. Experts can observe human motion and make interpretations and conclusions based on their knowledge (Simon 2004). In the ingress motion, however, one often needs to observe a large number of joints moving simultaneously in a three-dimensional setting. Using visual observation to identify motion patterns can thus be ineffective and time consuming, and the results are often highly subjective.

Another possible way to identify motion patterns is to use traditional feature extraction methods such as principal component analysis (PCA). However, PCA cannot be directly applied to human motion data due to its multistream structure. One way to overcome this issue is to stack up the multistream trajectories into one high-dimensional vector and then apply PCA, which is called stack-up PCA (Bharati *et al.* 2004). As human motion data possess a complex temporal and spatial correlation, applying this method on the ingress motion data will break down the correlation structure. It is therefore desirable to develop an effective feature extraction method that can be applied

to human motion data without altering its multistream structure.

Lu *et al.* (2009) proposed a dimension reduction and feature extraction method called uncorrelated multilinear principal component analysis (UMPCA) for multistream waveform signals with a higher-order tensor representation structure. Similar to PCA, UMPCA produces uncorrelated features; however, UMPCA can be applied to multistream data, thus preserving the structure of human motion data. This research proposes a method that uses UMPCA to automatically identify important variation patterns in human motion data. In this dissertation, UMPCA is first applied to simulated data to show its superiority over stack-up PCA. Subsequently, UMPCA is applied to the ingress data to identify the major variation patterns in the ingress motion.

1.3.2 Predicting Subjective Responses Using Human Motion for Assessing Vehicle Ingress Design

The objective of this task is to propose a general modeling framework that can be used to develop a statistical model for predicting subjective ingress discomfort responses using ingress motion data. The biggest challenge in constructing such a model is the high dimensionality of motion curves. The underlying assumption in most statistical regression modeling methods is that the number of samples is higher than the number of variables (Bellman *et al.* 1961, Donoho 2000, Fan and Li 2006). In the current case, as in many situations with high-dimensional data, the number of potential predictors greatly exceeds the number of trials (samples or observations). This may lead to overfitting and unstable parameter estimates (Vapnik 1998, Jain *et al.* 2000). Moreover, if only a few variables are actually important for prediction, the remaining variables act as noise that increases the classification error (Fan and Fan 2008). Another challenge in analyzing

motion curves is their misalignments among different trials. This issue is inevitable because different participants may have different start/end locations and perform trials at different paces. Directly using such misaligned curves for analysis will produce misleading results (Ramsay and Li 1998).

To overcome the issue of high dimensionality, Dufour and Wang (2005) proposed a method that uses joint angles, instead of motion curves, to evaluate ingress discomfort. This method is based on the concept of "neutral movement," where deviations from neutral joint angles are assumed to be associated with ingress discomfort. This approach, however, requires a priori judgment regarding the joints that are important for predicting ingress discomfort. These judgments rely mostly on intuition rather than data, which may not always lead to meaningful results. Moreover, because this method only uses joint angles to assess ingress discomfort instead of human motion trajectory data, it does not fully utilize human motion information.

In this research, several steps are taken to overcome the challenges of misalignment and high dimensionality. To address the issue of misalignment, right and left ankle trajectories are used to align motion curves using the right-leg-first strategy (Chateauroux 2009). To address the issue of high-dimensional motion data with a limited number participant-tests, a two-step data dimension reduction approach is proposed. The first step is to reduce the data dimension of each trajectory profile by parameterizing the profile data with B-spline basis functions (De Boor 1978). The second step is to identify the trajectories that are important for predicting participants' discomfort ratings. For this purpose, two group variable selection methods, group nonnegative garrote (GNNG) (Yuan and Lin 2006) and stepwise group selection (SGS), are employed. GNNG is used

to filter out non-relevant trajectories, and SGS is used to further select the more important trajectories for building the prediction model. Based on the selected trajectories and B-spline coefficients, a classification and prediction model is built using support vector machine (SVM) (Cortes and Vapnik 1995). The performance of the proposed framework is then evaluated against simpler prediction models, such as using vehicle design variables and anthropometric data to predict ingress discomfort.

1.3.3 Sample Size Calculation for a Functional Human Motion Analysis

Using the method proposed in Section 1.3.2, subjective ingress discomfort responses can be predicted from ingress motion data. In some cases, however, manufacturers are interested in the proportion of participants who rated the ingress discomfort of a vehicle design above some threshold, referred to as *response proportion* (RP). The objective of this task is to develop a method that can enable statistical testing of the RP of two vehicle designs; this includes hypothesis testing to examine whether the RP of one design is significantly higher than the RP of another and sample size calculation to determine the number of samples required to detect a difference in the RP of two designs given a specified power.

In literature, many methods have been developed to test whether there is a significant difference between two proportions (Newcombe 1998). Power calculations and sample size determination for testing the difference between proportions have also been studied (Faul *et al.* 2007, Cohen 2013). In these methods, the responses used to estimate the proportions are assumed to follow a binomial distribution. Although this assumption is appropriate for an RP that is estimated using subjective responses, it is not immediately apparent that this relationship can be used to estimate the standard deviation of an RP

predicted using human motion data due to the complex relationship between the motion model parameterization and the predicted subjective responses.

In this task, a dual-bootstrap approach is proposed to estimate the standard deviation of a proportion estimated using a prediction model, referred to as σ_{RP}. This dual-bootstrap approach enables us to calculate the two sources of variation in σ_{RP}. One is the modeling variation due to the uncertainty of the estimated prediction model (σ_m), and the other is the sampling variation due to randomly choosing test participants from the population (σ_s). The first bootstrap of this methodology is to generate the training datasets, called "bootstrap training datasets." These bootstrap training datasets are used to train prediction models using SVM classifiers, as done in the task outlined in Section 1.3.2 (Masoud *et al.* 2014). By training many SVM models, each with one bootstrap training dataset, we can capture the uncertainty in the prediction model, *modeling variance* (σ_m), which is due to the limited number of training samples. Afterwards, the second bootstrap is used to generate the prediction datasets, called "bootstrap prediction datasets." In contrast to the first bootstrap, this bootstrap enables us to capture the *sampling variance* (σ_s) due to the limited number of testing samples.

Chapter II
Analysis of Human Motion Variation Patterns Using UMPCA

2.1 Introduction

In recent years, increasing interest in the analysis of human motion data has been driven by a wide range of applications in different fields. In the athletics field, for example, Li et al. (2006) presented a multistep algorithm to automatically detect and recognize athletes' sporting actions in a long video with a dynamic background. Knudson (2013) introduced the concept of Qualitative Movement Diagnosis (QMD) to improve athletes' performance and reduce their risk of injury by visually observing video recordings of their motion. In the medical field, gait analysis, which uses motion data to analyze patients' walking patterns, is used to assist doctors' clinical diagnosis and treatment decisions. For example, Kay et al. (2000) discussed the impact of postoperative gait analysis on the assessment of treatment outcomes and planning ongoing care. In the automotive industry, Masoud et al. (2014) presented a systematic framework for using human ingress motion trajectories to predict customers' ingress discomfort ratings for improving vehicle design. Although these applications may have different objectives in terms of the usage of motion data, some common questions are often encountered during data analysis. For example, what are the typical motion variation patterns among different participants? Which time segments in a long video would be related to motion patterns of interest? Which particular joints and moving directions will reflect a normal or abnormal motion pattern of interest?

There are various ways to analyze human motion variation patterns. One simple way to analyze the motion patterns of tested participants is to replay recorded motion videos multiple times and use visual comparisons. For example, Cook et al. (2003) used gait analysis experts to visually compare 3D joint motion trajectories of patients with cerebral palsy with "normal" motion trajectories for assessing patients' need for surgery. This approach is effective when it is possible to clearly pre-define the normal motion pattern. However, in many other applications, such as vehicle ingress, the normal motion pattern of a comfortable design cannot be pre-defined. Moreover, the ingress motion data involve multiple joints moving in a 3D space. For example, Figure 2-1(a) shows the ingress motion trajectories of one trial (i.e., one participant testing one vehicle design) that are recorded at different joints such as ankles, elbows, and back vertebrae. Figure 2-1(b) shows a single joint's trajectory over time by connecting three moving directions (X, Y, and Z), which is referred to as a joint trajectory in this work. Thus, multiple joints' motions are referred to as multistream trajectory data. Considering such high-dimensional data, it is extremely cumbersome, if even possible, to extract the motion patterns among different participants by visually comparing the recorded motion videos of individual participants. Consequently, the conclusions regarding motion patterns based on visual comparison could be highly subjective. Therefore, an effective methodology to automatically analyze motion variation patterns is critically needed to reduce tedious data exploration efforts and avoid subjective bias.

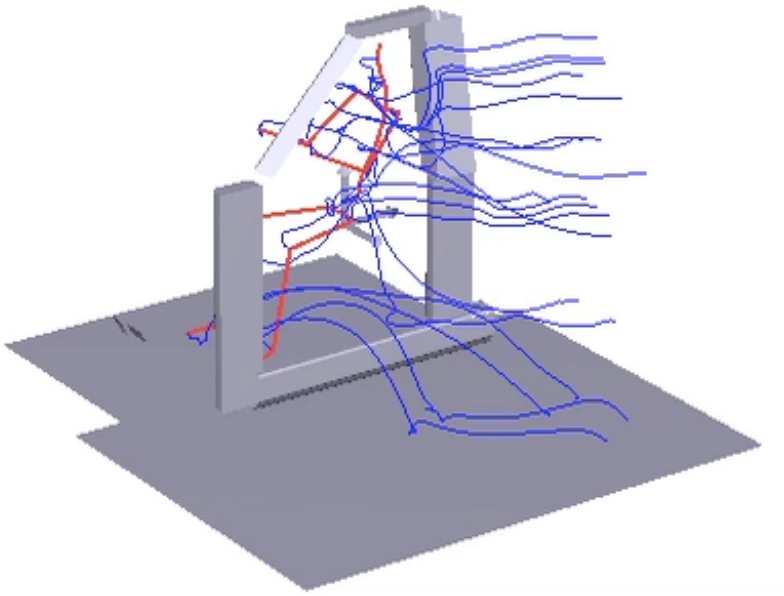

(a) Multi-stream trajectories

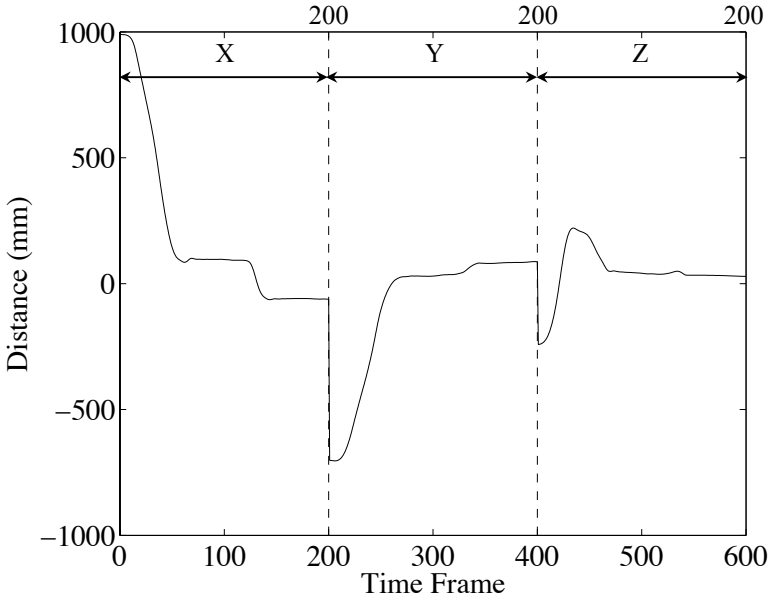

(b) The right ankle joint trajectory

Figure 2-1. Ingress motion data of one participant

Principal Component Analysis (PCA) is a commonly used method for analyzing multivariate variation patterns. If the analysis of motion data is based on a single trajectory, PCA can be applied directly. For example, the motion data of the right ankle joint trajectory shown in Figure 2-1(b) can be represented by a matrix, where each row vector represents the right ankle joint trajectory of one participant, and the number of rows represents the number of tested participants. It is impossible, however, to directly apply the conventional PCA method to multistream trajectories. One naïve way to apply PCA to such data is to combine the multistream trajectories into one high-dimensional vector before applying PCA. For example, if the ingress dataset has N tested participants with K joints recorded for each participant, and each joint trajectory has M data points, then the new dataset will be represented by a matrix of size $N \times MK$. PCA can subsequently be applied to this matrix to extract the significant variation patterns indicated by larger eigenvalues. A PCA analysis of this kind is known as stack-up PCA (Mason et al. 2001, Bharati et al. 2004). Using this stack-up method on human motion data would break down the spatial correlation structure among multiple joints and distort the temporal correlation within each joint. Several authors have already discussed the inefficacy of the stack-up PCA method in these situations (He et al. 2005, Paynabar et al. 2013, Yan et al. 2015). Therefore, an effective method for variation analysis that will not change the original multistream trajectory structure of human motion data is required.

In this chapter, a high-order array is used to represent the multistream trajectory data, and the Uncorrelated Multilinear Principal Component Analysis (UMPCA) method (Lu et al. 2009) is subsequently applied to analyze variation patterns in human motion. It is then shown that using a high-order representation followed by the UMPCA method can

preserve the original spatiotemporal correlation structure of the multistream structured data; therefore, it can provide more efficient dimension reduction and feature extraction compared to the PCA method.

The remainder of this chapter is organized as follows. Section 2.2 provides a brief review of the UMPCA method and considers how this method can be used for human motion analysis. In Section 2.3.1, a simulation study is presented to demonstrate the superiority of the UMPCA method over PCA in capturing the variation of human motion patterns in multistream datasets. In Section 2.3.2, the use of UMPCA is illustrated for selecting a few important joints, directions, and time segments from massive ingress motion data, which contribute most significantly to motion variations among the tested participants. Section 2.4 provides concluding remarks.

2.2 Methods

2.2.1 Basic Notation of Multistream Algebra

This subsection introduces the basis of using a high-order tensor representation for multistream trajectory data. A tensor is a multidimensional array that can be used to represent data with more than two dimensions. Each dimension of a tensor is called a mode or order. A tensor is denoted by $\mathcal{X}^{I_1 \times I_2 \times \ldots I_N}$, where I_n (n = 1,…, N) indicates the number of elements in the n^{th} mode. For example, human motion data can be represented by a third-order tensor denoted by $\mathcal{X}^{K \times M \times N}$, where K, M, and N are the number of elements in the joint, trajectory, and participant modes, respectively. Although there are different ways of projecting a tensor to a vector, this research focuses on the tensor-to-vector (TVP) method introduced by Lu et al. (2009). Briefly, TVPs are multiple projections of a tensor-to-scalar yielding a vector. In each projection, the TVP method

projects the matrix of K-joints' trajectories for each participant to a scalar using Elementary Multilinear Projections (EMPs). An EMP is used in a series of mode-r tensor-to-vector products with r = 1, 2. In other words, the second-order tensor representing each participant's K-joints' trajectories can be projected to a scalar z as $z = \mathcal{X} \times_1 v_p^{(1)^T} \times_2 v_p^{(2)^T}$, where $v_p^{(1)^T} \in R^K$ and $v_p^{(2)^T} \in R^M$ are the p^{th} projection vectors corresponding to the modes of the joint and trajectory, respectively. If P EMPs are considered for projection, these EMPs can be sequentially used for tensor-to-scalar projections. As N participants are performing the ingress motion, using P EMPs leads to N projected (transformed) vectors:

$$z^n \in R^{P \times 1} = \left\{ \mathcal{X} \times_1 v_p^{(1)^T} \times_2 v_p^{(2)^T} \right\}_{p = 1,2 \dots P} \text{ with } n = 1,\dots, N.$$

2.2.2 Uncorrelated Multilinear Principal Component Analysis (UMPCA)

Tensor decomposition has been widely studied in literature, and many techniques to factorize a tensor have been introduced. A detailed review on various decomposition techniques is presented in Kolda and Bader (2009).

This research aims to apply the UMPCA method proposed by Lu et al. (2009) to decompose the ingress data with the purpose of detecting the most critical segments of the motion. This section briefly elaborates upon the essentials of the UMPCA method. UMPCA takes advantage of the TVP method to project each tensor to a vector. Analogous to PCA, the objective of UMPCA is to obtain the EMPs (projection vectors) while maximizing the variance of projected vectors z^n's under some constraints that are discussed later on. The variability of the transformed vectors across the N samples can be computed as

$$s^p = \sum_{n=1}^{N}(z_p^n - \bar{z}^p)^2, \qquad p = 1, 2,\ldots,P \tag{2.1}$$

where z_p^n is the p^{th} component of vector z^n, and $\bar{z}^p = \frac{\sum_{n=1}^{N} z_p^n}{N}$. As mentioned before, each transformed vector z^n, n = 1, 2,…,N has P elements. Based on this fact, the p^{th} coordinate vector $g^p \in R^N$ can be obtained by choosing the p^{th} element of the transformed vectors z^n, n = 1, 2,…,N. Then, the objective function of the UMPCA technique can be defined as

$$\left\{v_p^{(r)^T} \; r = 1,2\right\} = \text{argmax}\, s^p = \sum_{n=1}^{N}(z_p^n - \bar{z}^p)^2 \tag{2.2}$$

Subject to

$$v_p^{(r)^T} v_p^{(r)} = 1, \qquad r = 1,2 \qquad p = 1, 2, \ldots, P$$

$$\frac{g^p g^q}{\|g^p\|\|g^q\|} = 0,\ p \neq q = 1,2 \ldots P \tag{2.3}$$

In summary, by exploiting P EMPs, UMPCA takes the ingress motion tensor $\mathcal{X}^{K\times M\times N}$ and projects it to a low-dimensional subspace in R^p, where $P < \min[K, M, N]$ (Lu et al. 2009). Unfortunately, there is no closed form solution to this problem. One common approach to solve this problem is to assume that the projection vectors for all modes are pre-known except for one mode and solve the problem for that mode. Then, this procedure is repeated iteratively until convergence. A detailed algorithm to solve the objective function defined in Eq. (2.3) is provided by Lu et al. (2009). The relative importance of each EMP can be evaluated as the ratio of the explained variance by that EMP to the total explained variance, i.e.,

$$R_p = \frac{s^p}{\sum_{p=1}^{P} s^p} \times 100\%, \tag{2.4}$$

where R_p is the relative importance metric for the p^{th} EMP, and s^p is the variance of the p^{th} transformed. The p^{th} eigentensor for the mode of the joint and trajectories can be defined as

$$V_p^{(1,2)} \in R^{K \times M} = v_p^{(1)} \circ v_p^{(2)}, \tag{2.5}$$

where $v_p^{(1)} \circ v_p^{(2)}$ is the outer product of the projection vectors of the joint and trajectory. These eigentensors combine all the information provided by the projection vectors in the selected modes.

2.3 Results

2.3.1 Performance Comparison Between PCA and UMPCA Using Simulation

This section presents a simulation study that was conducted to show the advantage of using UMPCA over PCA for tensorial data. For this purpose, a set of surrogated tensorial data was generated based on real ingress motion profiles, which are represented by a third-order tensor $\mathcal{Y}$. Mode 1 represents the different joints; Mode 2, the joint trajectories; and Mode 3, different participants. The motion data of K = 4 joints for N = 100 participants are simulated. Each joint is represented by a trajectory with M = 600 points, of which 200 points represent each of the directions X, Y, and Z. An element in tensor $\mathcal{Y}$ is denoted by y_{ijk} (i = 1,…, 4; j = 1,…, 600; k = 1,…, 100), which corresponds to the j^{th} point on the trajectory of joint i with regard to participant k.

The purpose of this simulation is to illustrate how UMPCA is used to systematically find important joints capable of representing and inferring the major motion variation patterns. The simulation condition is set such that Joint 1 has the highest variability

among all other joints, Joint 2 has the second largest variance, and Joints 3 and 4 have exactly the same variance, i.e., $\sigma_{j_1}^2 > \sigma_{j_2}^2 > \sigma_{j_3}^2 = \sigma_{j_4}^2$, where $\sigma_{j_i}^2$ is the variance of Joint i. Furthermore, Joints 1 and 2 are positively correlated, whereas Joints 3 and 4 are negatively correlated. The joint trajectories are simulated by using a mixed-effect model that is defined as

$$Y^{(k)} = X(B + R) + E \tag{2.6}$$

where $Y^{(k)}$ is the M×K matrix of the trajectories for the k^{th} participant, i.e., the i^{th} column of matrix $Y^{(k)}$ gives the trajectories of the i^{th} joint for participant k. X is the M×L matrix of B-spline basis values with L knots. A more realistic simulation dataset is obtained by using surrogate B-spline coefficients, which were obtained from real ingress trajectories, to generate the simulated trajectories, in which the trajectory of each joint is reconstructed using L = 9 knots. The matrix of fixed-effect coefficients is denoted by $B \in \mathbb{R}^{L\times K}$ and that of random effect coefficients, by $R \in \mathbb{R}^{L\times K}$. Each row in matrix R is normally distributed with a zero mean vector and a covariance matrix $U \in \mathbb{R}^{K\times K}$; the elements of matrix U can be obtained based on the variability of each joint and the covariance between different joints. Furthermore, matrix $E \in \mathbb{R}^{M\times K}$ is the vector of random errors following a normal distribution with a zero mean vector and a diagonal covariance matrix $\sigma_\varepsilon^2 I$ with $\sigma_\varepsilon^2 = 0.5$. The random-error matrix E is assumed to be independent of the random-effect matrix R.

The generation of the simulation trajectories enables us to compare the UMPCA and PCA results to determine which method can more effectively capture the variation of motion patterns and the cross-correlation among different trajectories. Specifically, upon applying the UMPCA method to the simulated data, the relative importance R_p of the

first four components was 54.62%, 32.09%, 11.19%, and 2.09%, respectively. Because the first two components are the most important, this analysis focuses on these two components.

Figure 2-2 shows the first and second eigentensors of the UMPCA method. Figure 2-2(a) indicates that the first eigentensor assigns higher weights to Joints 1 and 2 and almost zero weights to Joints 3 and 4. The weights of the first joint are slightly larger than those of the second joint during the whole motion. This shows consistency with the simulation condition of $\sigma_{j_1}^2 = 1000$, $\sigma_{j_2}^2 = 900$, and $\sigma_{j_3}^2 = \sigma_{j_4}^2 = 300$. Moreover, as the variability of Joints 3 and 4 is smaller than that of Joints 1 and 2, the first eigentensor only focuses on the prevalent Joints 1 and 2. Figure 2-2(b) shows the second eigentensor; it suggests a contrast between Joints 3 and 4, which is quite obvious when considering the motion in its entirety. This verifies the strong negative correlation $\rho_{j_3 j_4} = -0.8$. Figure 2-3 shows the first and second eigenvectors of the joints mode obtained by UMPCA. As expected, in the first eigenvector, Joints 1 and 2 have higher weights compared to those of Joints 3 and 4. In the second eigenvector, it is clear that Joints 3 and 4 have the highest weights with opposite signs, highlighting the negative correlation between these joints.

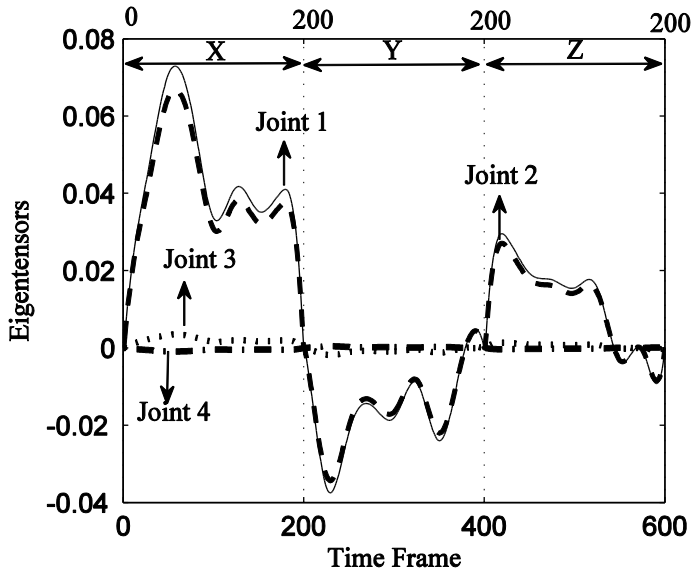

(a) First eigentensor

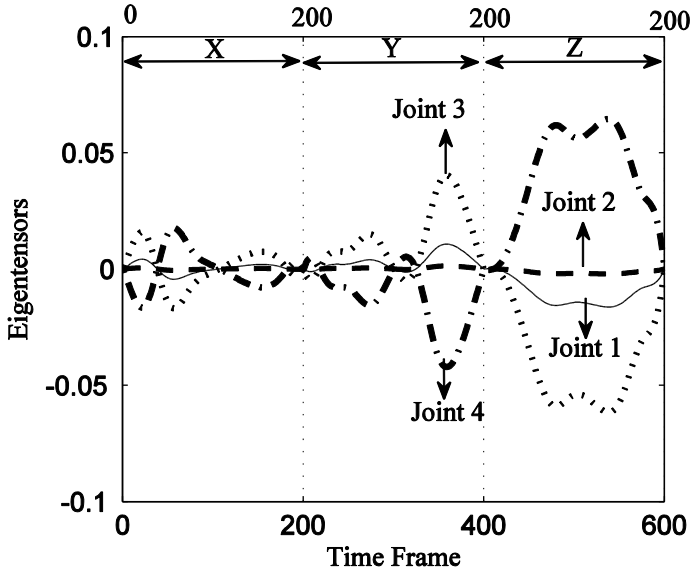

(b) Second eigentensor

Figure 2-2. UMPCA eigentensors

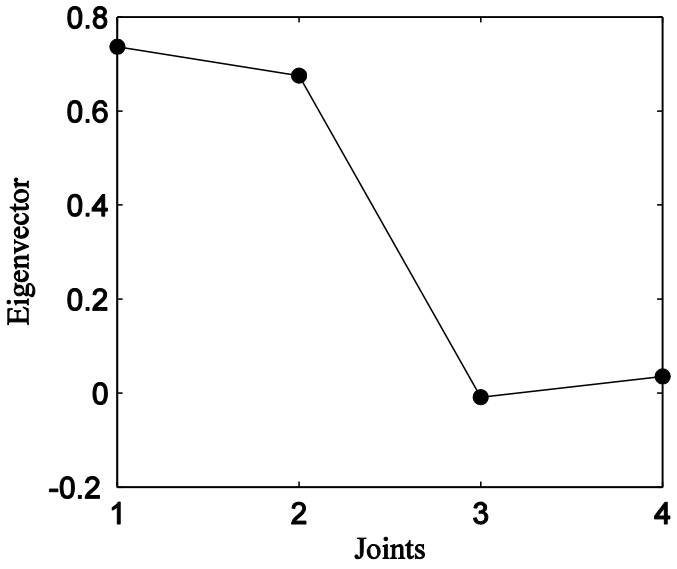

(a) First eigenvector

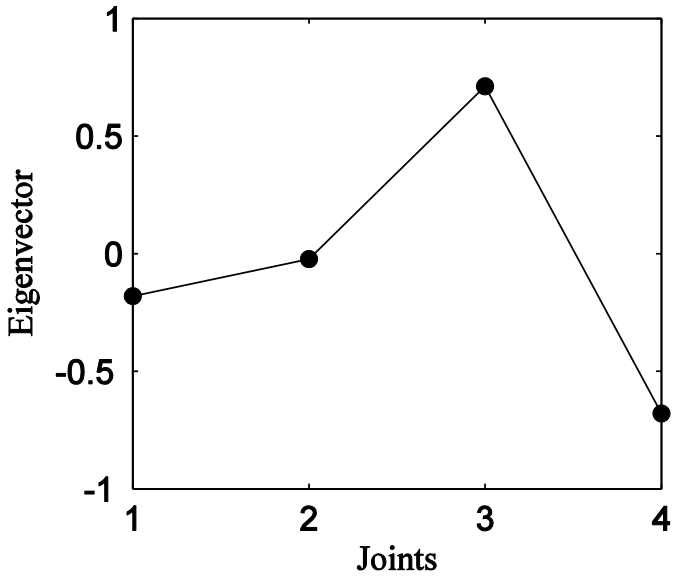

(b) Second eigenvector

Figure 2-3. UMPCA joint mode eigenvectors

For the comparison between the UMPCA and the PCA methods, we further apply the PCA method to the same simulated dataset. The resultant relative importance of the first four PC components is 29.04%, 28.66%, 22.36%, and 19.95%, respectively. Figure 2-4 shows the first and second eigenvectors as computed by the PCA method. It is noticeable in Figure 2-4(a) that there is no consistent significant joint that always show a higher weight than others. For example, although Joints 1 and 2 have higher weights in the X-direction, Joint 3 has higher weights in some portions of the Y-direction. Accordingly, we cannot conclude that only Joints 1 and 2 significantly contribute to the first eigenvector in all three directions.

Figure 2-4(b) shows the second eigenvector of the PCA method. This eigenvector, similar to the first eigenvector estimated by PCA, emphasizes the importance of Joints 1 and 2, unlike the UMPCA result that was able to clearly identify a new motion pattern that emphasizes the negative correlation between Joints 3 and 4. This simulation shows that the UMPCA method is more effective than PCA in analyzing multi-stream signals, especially in cases in which cross-correlations among signals exist.

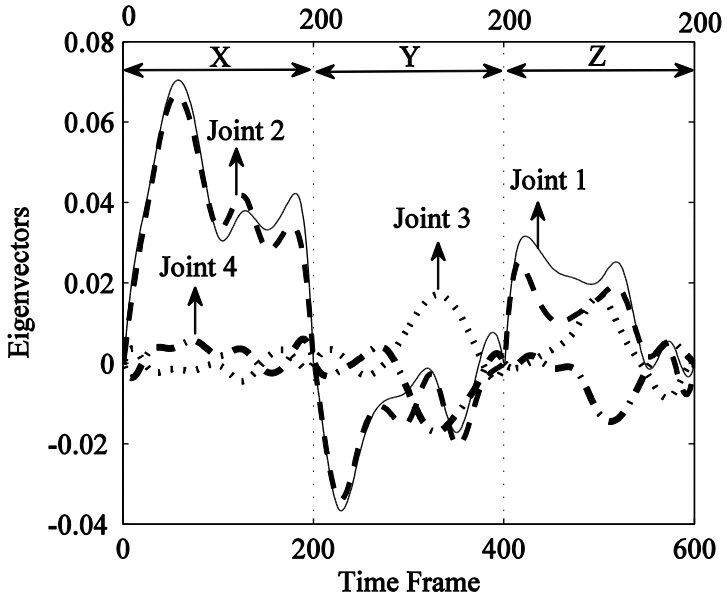

(a) First eigenvector

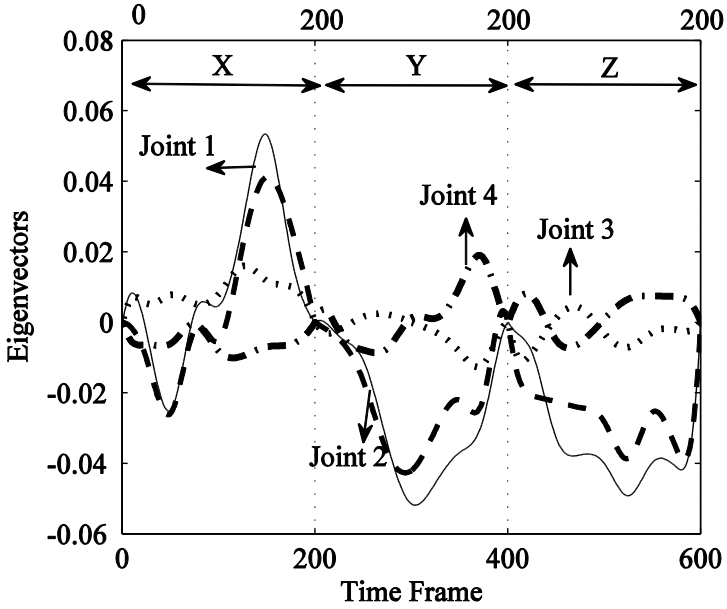

(b) Second eigenvector

Figure 2-4. First and second eigenvectors computed by PCA method

2.3.2 Case Study: Identifying Important Ingress Motion Patterns

In this section, the UMPCA method is applied to analyze experimental data relating to ingress motion. In this experiment, 15 participants with different anthropometric features were selected to perform vehicle ingress trials on two vehicle designs (i.e., 30 trials), of which one was comfortable to ingress and the other difficult, based on the ratings of tested participants. During the participants' movement, markers (tracking sensors) were attached to different locations on the participants' body to track the ingress motion. By using the information from the markers, the trajectories of 20 different joints were obtained. The trajectories of the 15 participants were registered using the right-leg-first strategy (Chateauroux 2009, Masoud et al. 2014). The trajectory data are represented by the third-order tensor $\mathcal{X}^{20\times600\times30}$, where the three tensor modes correspond to the joints, trajectories, and participants, respectively.

The UMPCA method was applied to this tensor data as a systematic way to automatically identify those motion patterns with high variation in the ingress motion and also to identify which motion pattern is associated with ingress comfort. Table 2-1 lists the relative importance of the first ten UMPCA components. It can be observed that the first UMPCA component is the most important component with a relative importance of 79.44%. Hence, our subsequent inference analysis only focuses on this first component.

Table 2-1. Relative importance of UMPCA components applied to human motion data

UMPCA Components	Relative Importance
1	79.44%
2	12.75%
3	4.31%
4	1.30%
5	0.90%
6	0.47%
7	0.31%
8	0.25%
9	0.12%
10	0.05%

Figure 2-5 shows a plot of the eigenvector weights of the first component obtained using UMPCA. The joint mode eigenvector shown in Figure 2-5(a) shows the joint contributions among 20 joints, and the trajectory mode eigenvector shown in Figure 2-5(b) shows the importance among time frames 1–200 in each of the X-, Y-, and Z-directions. The important joints and time frames that significantly contribute to the UMPCA component are systematically identified by applying the hierarchical clustering method (Hastie *et al.* 2009) to each eigenvector. This clustering method determines the decision boundaries to automatically remove unimportant small weights in each eigenvector, which fall within the shadow region in Figure 2-5. Specifically, Figure 2-5(a) shows that only 8 joints (i.e., head, neck, T1T2, right shoulder, left shoulder, right clavicle, left clavicle, and left elbow) are important joints beyond the shadow region. Figure 2-5(b) shows that only the time frames 97–132 in the X-direction and 42–200 in

the Z-direction are important. This is explicitly interpreted to indicate that the first UMPCA component mainly represents the motion of the upper body in the longitudinal and vertical moving directions as the participant lower their head to enter the vehicle. Moreover, Figure 2-5(b) can further facilitate the identification of the specific time frames in which this motion pattern is most evident (i.e., the most significant variation pattern in the X- and Z-direction occurs at time frame $t_x^* = 111$ and $t_z^* = 79$, respectively).

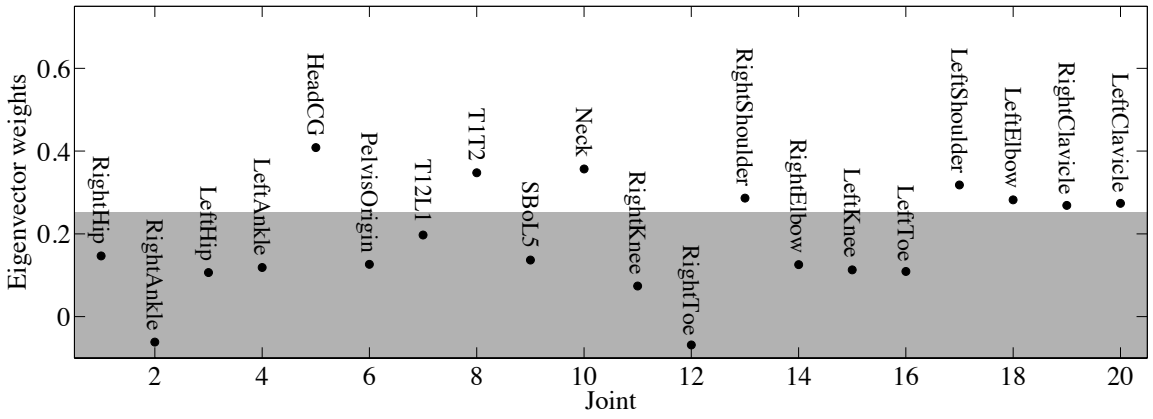

(a) First eigenvector – joint mode

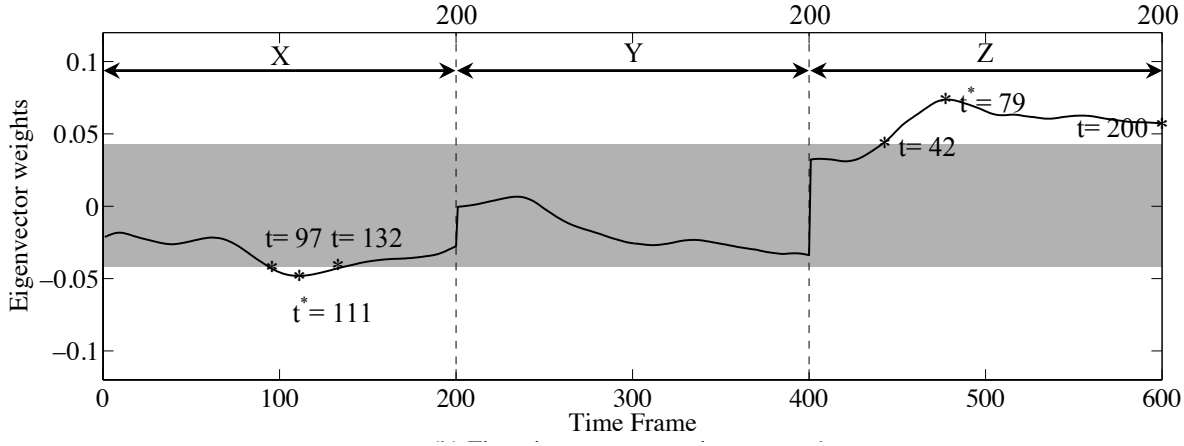

(b) First eigenvector – trajectory mode

Figure 2-5. Eigenvectors of the first UMPCA component

We verified these facts by plotting several time frames of one participant performing the ingress motion for both vehicles in Figure 2-6 and Figure 2-7, respectively, where the selected time frames correspond to the points identified in Figure 2-5. We can observe that Figure 2-6 shows inference results consistent with those of Figure 2-5, that is, the most significant variation between the upper body joints in the X-direction occurs at time frames 97–132. In this case, the variation at $t_x^* = 111$ is similar to that at time frames 97 and 132 due to their similar eigenvector weights. Similarly, Figure 2-7 shows that the most significant variation in the Z-direction occurs during time frames 42–200 and is most evident at $t_z^* = 79$. This shows the advantage of using the UMPCA method, which obviates the need for tedious visual efforts in finding the specific time frames of the most significant motion patterns.

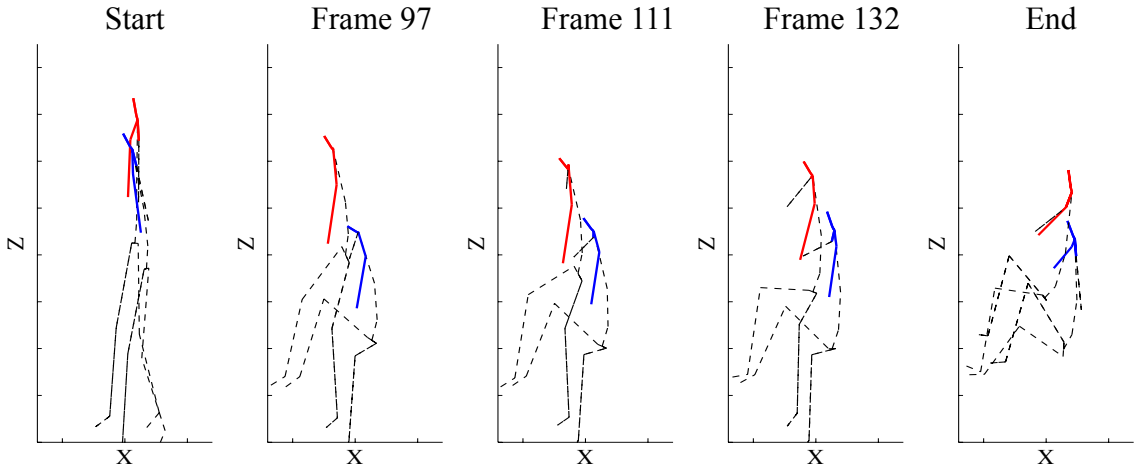

Figure 2-6. Ingress motion – joints and time frames identified by the first UMPCA component in the X-direction

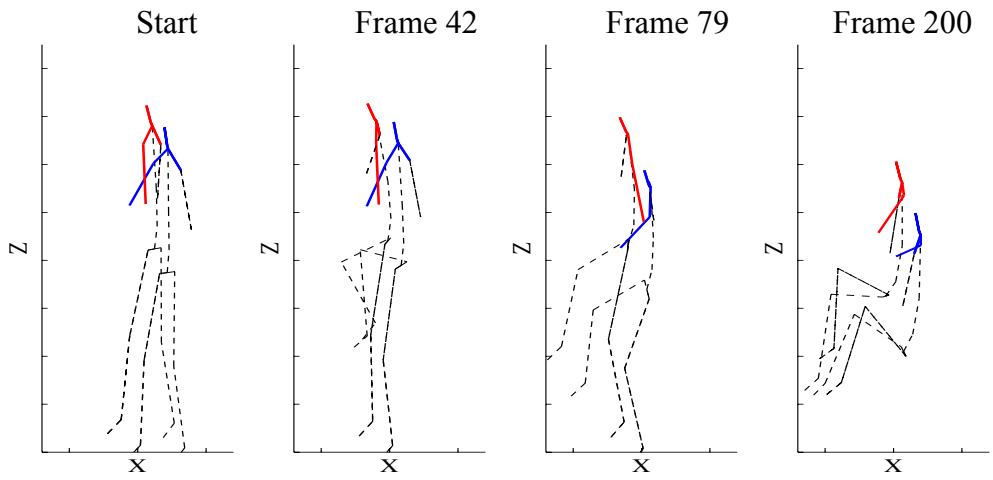

Figure 2-7. Ingress motion – joints and time frames identified by the first UMPCA component in the Z-direction

The effect of the first motion pattern on discomfort was studied by plotting the UMPCA scores of the first and second UMPCA components (Figure 2-8). The scores associated with the first vehicle design, which has a comfortable ingress, are denoted by crosses, and the scores associated with the second vehicle design, which has a less comfortable ingress, is denoted by circles. It can be observed that the first UMPCA component clearly separates the two vehicle designs, thus showing that the first motion pattern has a strong effect on the ingress comfort. This information enables vehicle designers to study the vehicle design parameters that have an effect on this motion pattern, and implement design changes to improve ingress comfort.

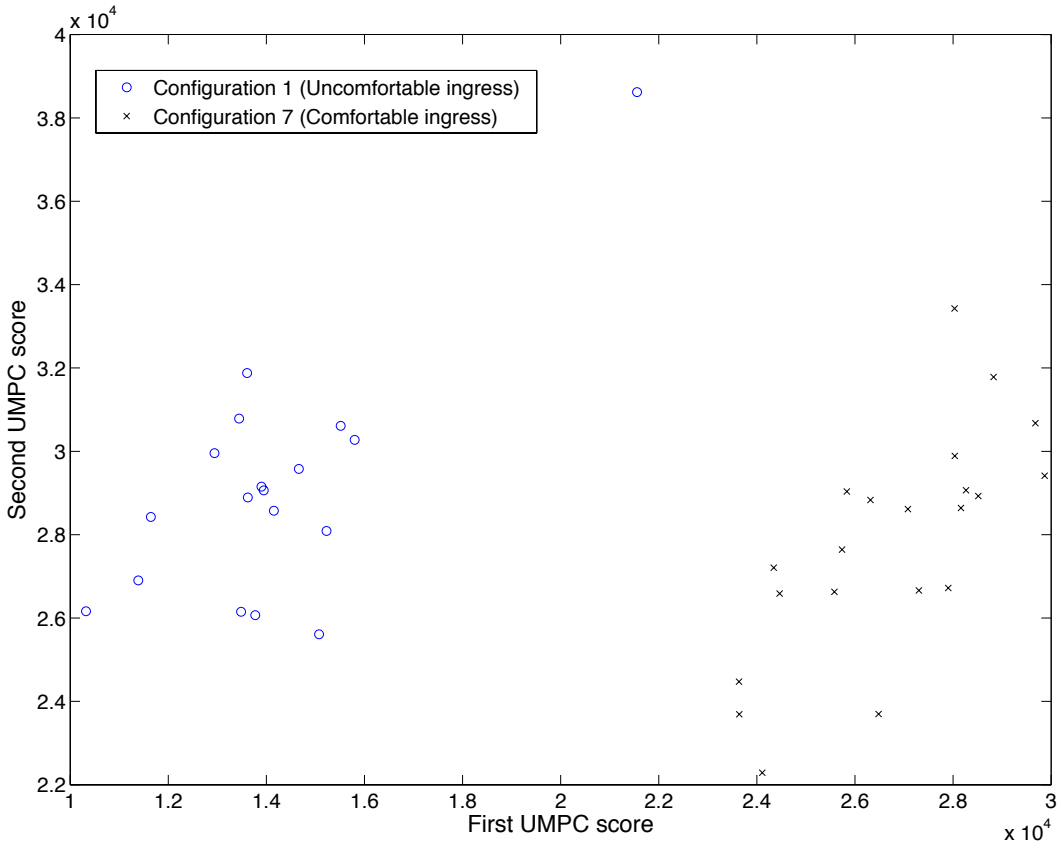

Figure 2-8. First and second UMPCA scores for two vehicle configurations

To further investigate the relationship between the first motion pattern and the ingress comfort rating, the motion data of all 17 vehicle configurations were projected on the first and second UMPCA components. Figure 2-9 shows the mean score per configuration for the first and second UMPCA components. We can observe that vehicles with high comfort ratings (ex. Conf. 7 and 11) are associated with high UMPC 1 scores, while vehicles with low comfort ratings (ex. Conf. 1 and 8) are associated with low UMPC 1 scores. This result is consistent with Figure 2-10, which plots the first UMPC scores against the ingress comfort ratings per vehicle. We can also observe from Figure 2-11 that the second UMPCA pattern is not highly associated with ingress comfort ratings.

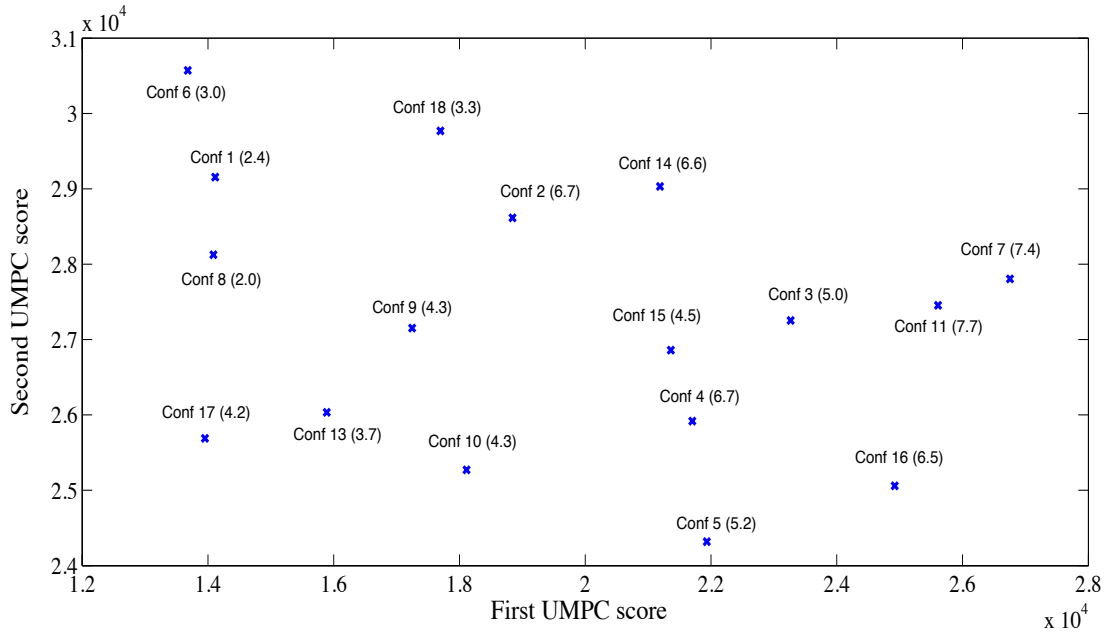

Figure 2-9. Mean scores of different vehicle configurations on the first and second UMPCA components (mean ingress comfort rating in parenthesis)

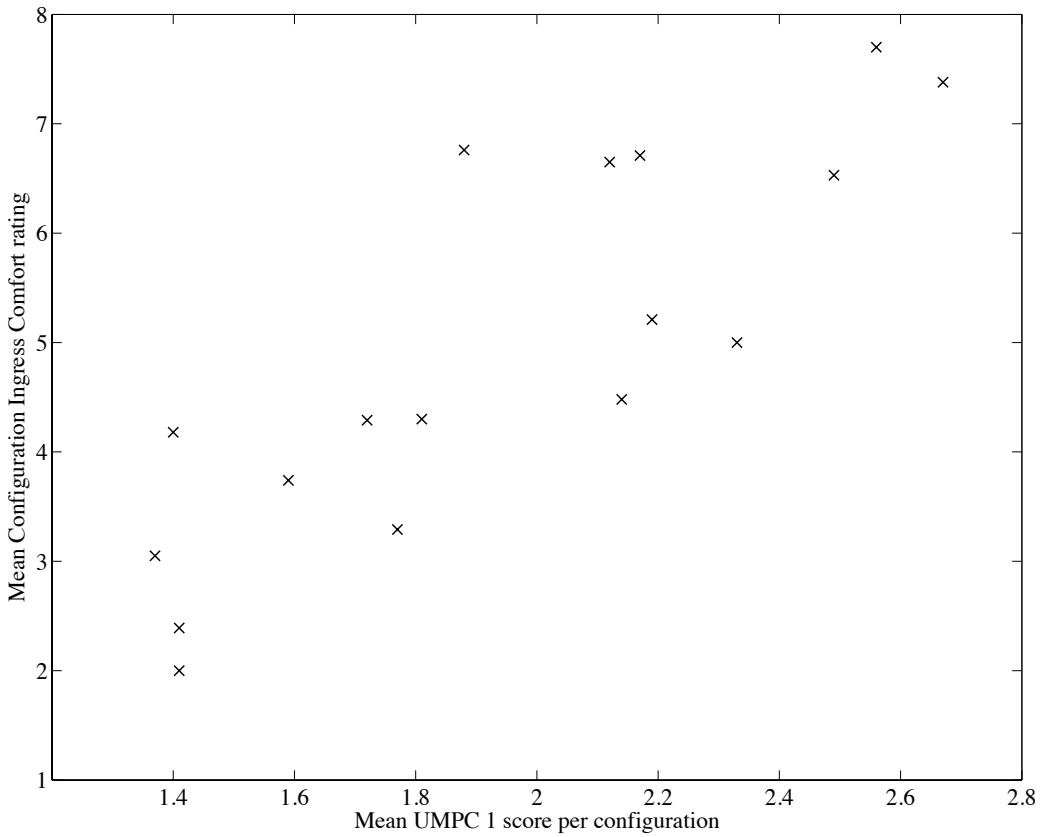

Figure 2-10. Mean score of the first UMPCA component vs. mean ingress comfort rating

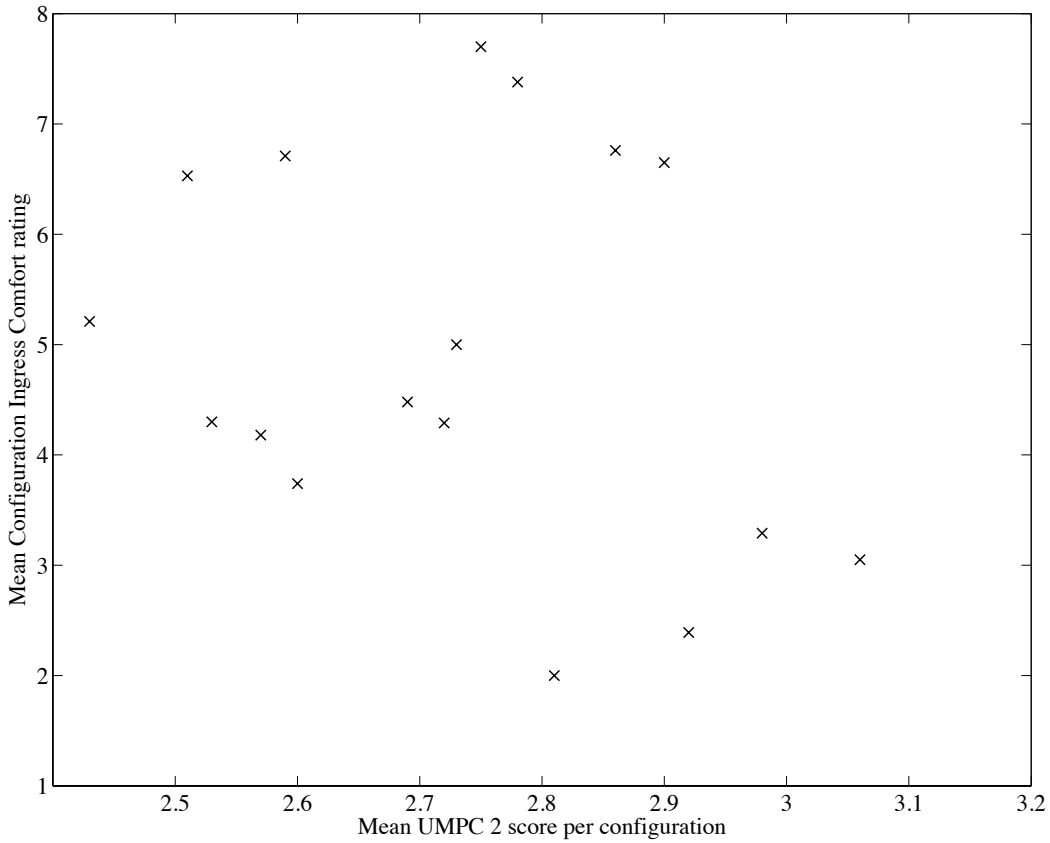

Figure 2-11. Mean score of the second UMPCA component vs. mean ingress comfort rating

2.4 Conclusion

This chapter proposes a method for identifying important human motion variation patterns using UMPCA. Unlike PCA, this method preserves the multistream structure of the motion data. A simulation study was conducted to demonstrate the superiority of UMPCA over PCA. The simulation results showed that UMPCA can capture the cross-correlation among different signals and important variation patterns more effectively than PCA. UMPCA was also applied to a case study for vehicle ingress motion analysis, where the motion pattern that has the highest variation was identified. We further demonstrate that this motion pattern is associated with ingress discomfort, although this

may have been a coincidence due to the particular test conditions selected. The information about this motion pattern can be used to guide and improve vehicle design.

This work involved the acquisition of human motion data using marker-based technologies, as explained in the introduction. The proposed method, however, is not restricted to marker-based trajectory data; rather, it can also be applied to other types of multistream trajectories. For example, markerless motion capture systems (Corazza et al. 2006) have provided an opportunity to capture human motion trajectories without using markers. Moreover, advances in computer vision technologies (Wang et al. 2003) have also enabled the capture of human motion trajectories using cameras that are not necessarily located in an experimental setting, such as surveillance cameras.

The proposed method can also be applied to various other human motion datasets such as those representing athletic performance evaluation and training, medical diagnosis, and video surveillance. This method can also be integrated into Gait analysis software packages to produce more consistent and reliable results for clinical diagnosis. In the future, we plan to develop a UMPCA-based method capable of producing sparse eigenvectors. This could further enhance the interpretability of the eigenvectors.

Chapter III
Predicting Subjective Responses Using Human Motion For Assessing Vehicle Ingress Design

3.1 Introduction

The discomfort associated with the ingress motion has increasingly become one of the important ergonomic factors considered in vehicle design (Wegner *et al.* 2007). Many methods have been proposed in literature to assess ingress discomfort. For example, earlier studies (Bottoms 1983, Petzäll 1995) used the time required for entry as the main discomfort measure, under which optimal vehicle design parameters were recommended to reduce entry duration. Kim and Lee (2009) developed a method that uses muscle forces to predict discomfort during ingress, in which fuzzy logic was used to establish the relationship between muscle forces and discomfort. Other studies were conducted to understand the relationship between vehicle design parameters and ingress discomfort. Giacomin and Quattrocolo (1997) analyzed the discomfort of ingress/egress into the rear car seat under different design parameters of the doorframe and seat, where discomfort was assessed using subjective responses. Causse *et al.* (2012) assessed the effects of roof height on ingress/egress discomfort using subjective responses. Although these studies took into account vehicle design parameters, they did not consider the effect of participants' movement variability.

Dufour and Wang (2005) proposed the concept of "neutral movement," which uses joint angles to assess discomfort during ingress/egress. The joint angles in this study were calculated from ingress/egress motion data obtained using motion capture systems. . This study, however, was limited to using joint angles rather than using the whole ingress motion.

Recent advancements in human motion simulation technology have provided vehicle engineers the ability to simulate drivers' ingress/egress motion before physical prototypes are made. These simulations can efficiently generate motion data of participants with a wide range of body sizes. However, few researches have modeled the relationship between ingress discomfort and human motion data.

Understanding the relationships between drivers' discomfort and their ingress/egress motion has several purposes. First, it helps guide vehicle design to reduce ingress difficulty. Second, it provides the potential capability of using computer-based simulations of ingress movements to predict subjective responses. This will reduce the need to conduct human participant-tests, thus reducing the cost and time required to assess the ingress discomfort of new vehicle designs. Third, subjective responses could be predicted in situations in which motion data can be obtained but soliciting subjective responses is not feasible or desirable.

This chapter presents a modeling framework that predicts subjective discomfort responses using ingress motion data, described by the Cartesian trajectories of body landmarks, known as *motion curves*. The biggest challenge in constructing such a model is the high dimensionality of motion curves. The underlying assumption in most statistical regression modeling methods is that the number of samples is higher than the

number of variables (Bellman *et al.* 1961, Donoho 2000, Fan and Li 2006). In the current case, as in many situations with high-dimensional data, the number of potential predictors greatly exceeds the number of trials (samples or observations). This may lead to overfitting and unstable parameter estimates (Vapnik 1998, Jain *et al.* 2000). Moreover, if only a few variables are actually important for prediction, the remaining variables act as noise that increases the classification error (Fan and Fan 2008).

Another challenge in analyzing motion curves is their misalignments among different trials. This issue is inevitable because different participants may have different start/end locations and perform trials at different paces. Directly using such misaligned curves for analysis will produce misleading results (Ramsay and Li 1998). Therefore, it is crucial to develop an effective modeling approach that can integrate curve alignment and data dimension reduction methods into the development of the prediction model.

The remainder of this chapter is organized as follows. Section 3.2 describes the data, framework, and methods used in this chapter. Section 3.3 presents the results of applying the framework to the ingress experiment data. Finally, Sections 3.4 and 3.5 present the discussions and conclusions.

3.2 Methods

3.2.1 Data Source

Ford Motor Co. performed a laboratory experiment to capture the motion of participants during the ingress and egress process. The 32 participants whose ingress and egress motions were captured are representative of the general population, ranging from a 3% female to a 98% male in height (stature). The participants also vary in weight and amount of body fat, ranging from very thin (BMI = 19) to obese (BMI = 52). Numerous

anthropometric measures were taken for each participant to ensure that a digital human manikin could be created in the future to accurately represent the participants.

The ingress and egress motions were captured for 17 vehicle package dimensions. The experiment was designed to ensure that 7 key design variables were varied to include values that not only are representative of vehicles currently in production but also go beyond those in existing vehicles to allow greater ranges for future models. These 7 design variables are shown in Figure 3-1 and are defined as per the SAE J1100 standard. Moreover, the Cartesian coordinate system used for this analysis was based on the SAE J187 standard coordinate system used in vehicle engineering. A programmable vehicle buck, the Human Occupant Package Simulator (HOPS), was used to create the vehicle packages. The HOPS includes integrated Vicon motion capture cameras that were strategically located to avoid obstructions between the cameras and body markers.

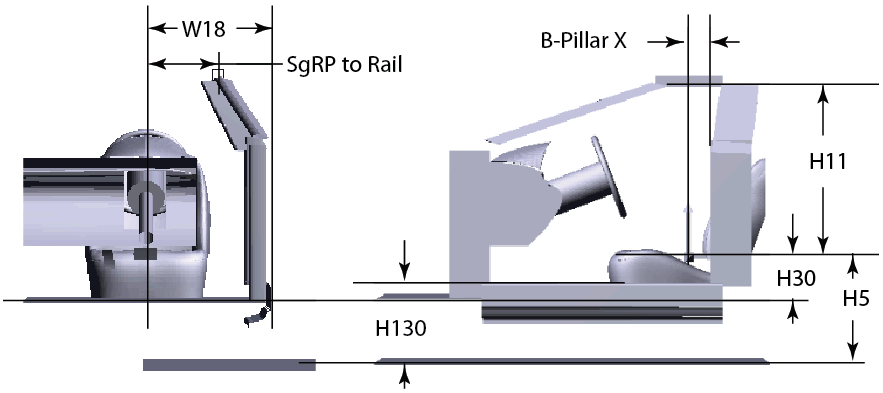

Figure 3-1. Car seat design variables

A unique set of reflective markers was designed to capture whole-body motion. The markers were attached to both anthropometric landmarks as well as in clusters to some segments (such as the thigh) to ensure that joint motions could be reconstructed accurately. Most markers were placed directly on the participant's skin to ensure that the motion of the bony structure and not that of the clothes was captured. Using custom

software, the trajectories of these markers were used to estimate the locations over time of 20 joints that define the kinematic linkage of the body. The 20 joints calculated are the right ankle, right knee, right toe, right shoulder, right elbow, right wrist, right clavicle, left hip, left ankle, left knee, left toe, left shoulder, left elbow, left wrist, left clavicle, head, neck, and the spinal vertebrae T12L1, T1T2, and S1L5. These joints were calculated because they were sufficient to define the whole-body kinematic linkage. Following the standard automotive industry convention, the trajectories were expressed in a coordinate system with the z axis (vertical), x axis (oriented fore and aft along the vehicle longitudinal axis), and y axis ("cross car").

After participants completed an ingress/egress trial, they were asked to rate the trial. The participants were asked the following question: "Please rate the ease of getting in and out of this vehicle configuration." The possible responses on a 10-point scale were 1–2 (unacceptable), 3–5 (average), 6–8 (outstanding), and 9–10 (truly exceptional). For the current analysis, these responses were transformed into 0/1 responses using thresholds (cutpoints), such as transforming a response to 1 if the rating was greater than 5.

3.2.2 Modeling Framework

The proposed modeling framework consists of three major steps (Figure 3-2). The first step is to register the motion curves. This includes selecting motion trials that demonstrate a consistent strategy (Chateauroux 2009) and aligning/normalizing the motion curves. In the second step, the dimensionality of motion curves is reduced by using a hierarchical two-level approach. In the first level, each motion curve is fitted by using B-spline basis functions, which can effectively represent functional data with a small number of spline coefficients (Silverman and Ramsay 2005). In the second level,

the number of joints is reduced by integrating two commonly used variable selection approaches to design a classifier: the filtering approach and the wrap approach (Kohavi and John 1997). In this research, the filtering approach is based on group nonnegative garrote (GNNG), a group variable selection method that is used to filter out joints that are not important for predicting the subjective response. Subsequently, the wrap approach, based on the stepwise group selection (SGS) method, is used to identify more critical joints that closely affect the classification performance. In the third step of the proposed framework, the support vector machine (SVM) classifier model is trained and validated via the cross-validation method. The resultant model can then be used to predict subjective responses of future trials.

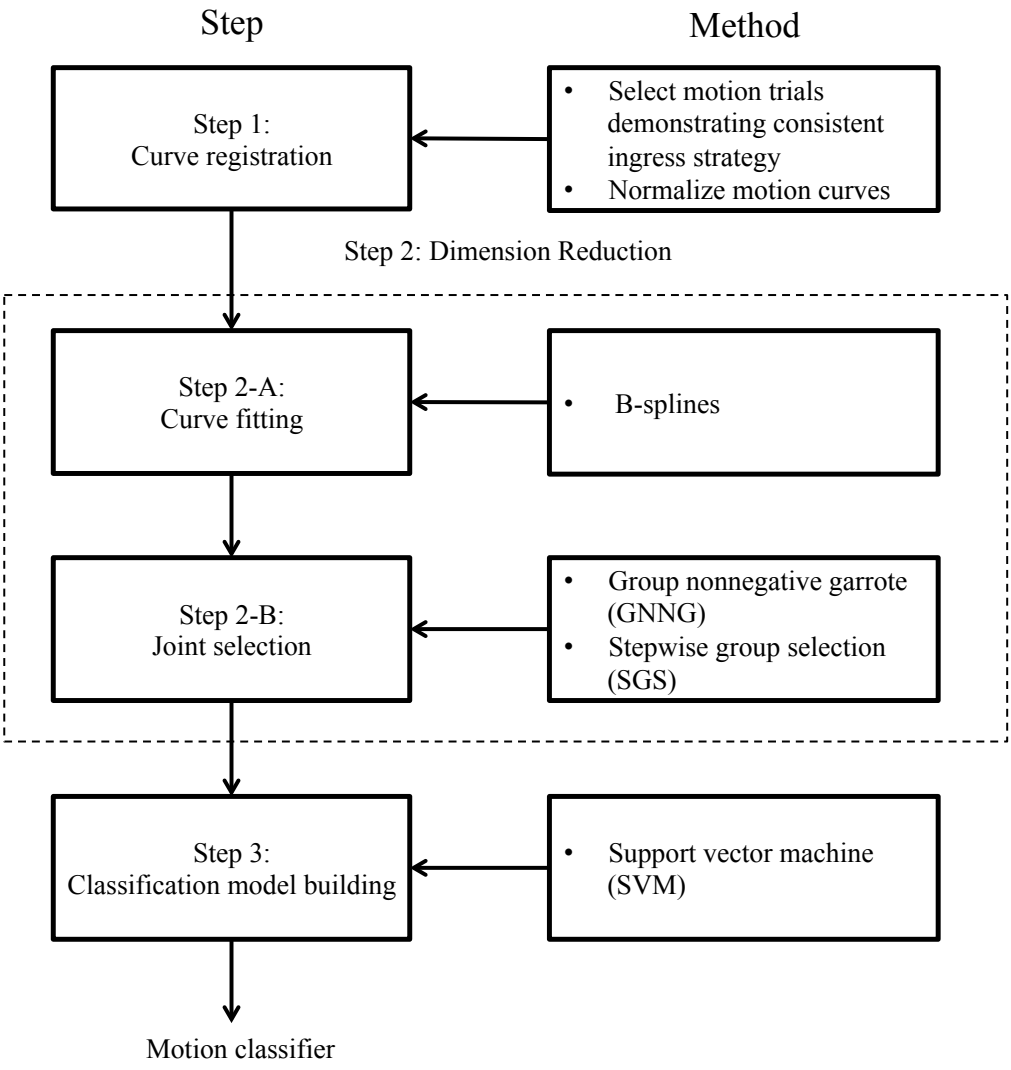

Figure 3-2. Framework for developing a classifier based on human motion

3.2.3 Step 1: Curve Registration

Curve registration aligns data in space and time so that particular features of the curves are colocated and that points on curves are compared at similar states (Ramsay and Li 1998). In this work, curve registration is conducted using two steps: defining the start/end points of each trial and normalizing the motion curves to have the same time range of [0, 1]. We have left the analysis of the motion duration for future work.

In the first step of curve registration, the right-leg-first strategy (Chateauroux 2009) was used to define the start/end points for ingress trial, i.e., each ingress trial starts when the right foot leaves the ground to enter the vehicle and ends when the left foot subsequently enters the vehicle. On the basis of this strategy, the speed signals of the right and left ankles can be used to identify the start/end point of ingress motion trials using the following rule: each trial starts at the beginning of the largest right ankle motion and finishes at the end of the largest subsequent left ankle motion. Figure 3-3 shows an example of using the right-leg-first strategy to define the trial's start/end points.

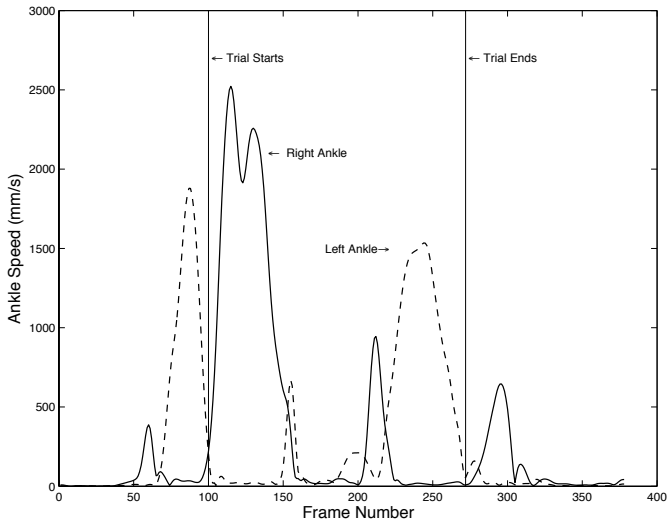

Figure 3-3. Define start/end points using the right-leg-first strategy

In the second step of curve registration, all motion curves are normalized to have the same time duration [0,1] so that signal shapes with different sampling durations (i.e., different number of frames) can be analyzed and compared more effectively (Silverman and Ramsay 2005). The duration of each trial was normalized by linear interpolation to the interval [0, 1] such that each curve contains exactly 200 frames. Linear interpolations were conducted as follows (Davis 1975):

Given that the number of frames in the original curve is (l_{old}) and the number of frames in the new curve is ($l_{\text{new}} = 200$) and

$$X_{\text{old}} = \left[0, \frac{1}{l_{\text{old}}-1}, \frac{2}{l_{\text{old}}-1}, \ldots, 1\right], \tag{3.1}$$

$$X_{\text{new}} = \left[0, \frac{1}{l_{\text{new}}-1}, \frac{2}{l_{\text{new}}-1}, \ldots, 1\right]. \tag{3.2}$$

The new curve is defined as follows:

$$y_{\text{new},i} = y_{\text{old},j} + \left(y_{\text{old},j+1} - y_{\text{old},j}\right)\frac{X_{\text{new},i} - X_{\text{old},j}}{X_{\text{old},j+1} - X_{\text{old},j}}, \text{ for } 1 < i < l_{\text{new}}, \tag{3.3}$$

$$y_{\text{new},1} = 0, \tag{3.4}$$

$$y_{\text{new},l_{\text{new}}} = 0, y_{\text{new},l_{\text{new}}} = 0 \tag{3.5}$$

where $y_{\text{old},j+1}$ and $y_{\text{old},j}$ are points on the original curve, and $y_{\text{new},i}$ is an interpolated point of the new normalized curve. The value of $X_{\text{new},i}$ is between $x_{\text{old},j+1}$ and $x_{\text{old},j}$.

Figure 3-4 and Figure 3-5 show an example of motion curves before and after registration, respectively. It can be observed that features are not aligned in Figure 3-4, whereas they are well aligned in Figure 3-5.

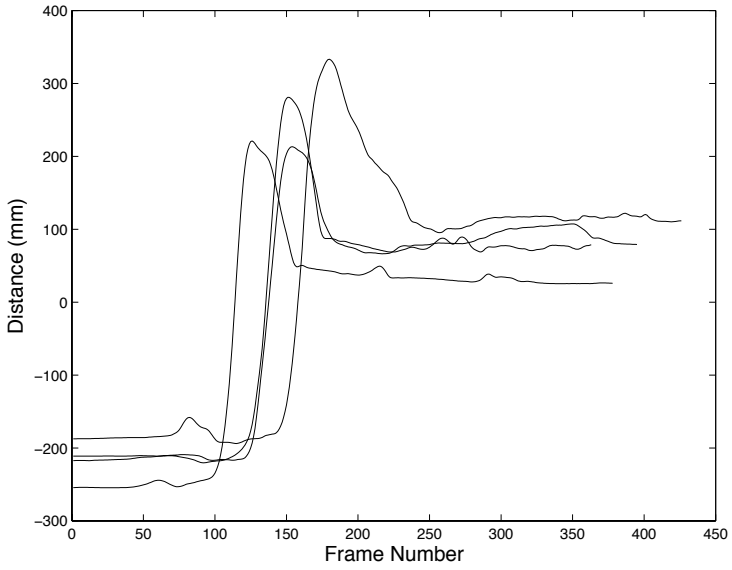

Figure 3-4. Example of right ankle curves (Z-direction) before registration

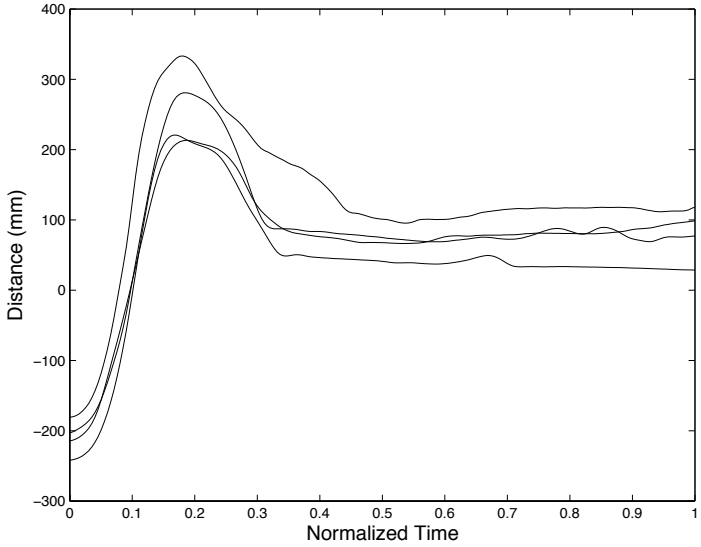

Figure 3-5. Example of right ankle curves (Z-direction) after registration

3.2.4 Step 2: Dimension Reduction

Step 2A: Individual Curve Fitting Using B-splines

In this methodology, a B-spline basis function (De Boor 1978) is used to fit the curves. A B-spline is a smooth polynomial function that can represent complex curves by

a small number of coefficients while preserving the basic features of the curve. B-splines are widely used in statistics to represent complex data (Cardot *et al.* 2004, Silverman and Ramsay 2005). The B-spline method was chosen in this framework to fit motion curves due to its simplicity of construction, accuracy, and ability to represent complex motion curves. Because the B-splines fit the trajectory curves closely, alternative curve fitting techniques with similar accuracy would likely have produced equivalent results. B-spline functions are mathematically defined as follows:

Let $T = \{t_0, t_1, t_2, \ldots, t_{m-1}\}$ be a nondecreasing sequence of m real numbers called *knots*. Then the linear combination,

$$C(t) = \sum_{i=0}^{n} P_i N_{i,p}(t) \tag{3.6}$$

is a B-spline curve with degree $p = m - n - 2$, where $P_0, P_1, \ldots, P_n$ are referred to as *control points* and the i^{th} B-spline basis function $N_{i,p}(t)$ is defined by the following recurrence relations:

$$N_{i,1(t)} \begin{cases} 1 & \text{if } t_i \le t \le t_{i+1} \\ 0 & \text{otherwise} \end{cases}, \text{ for } p = 1 \tag{3.7}$$

and

$$N_{i,p}(t) = \frac{t - t_i}{t_{i+p} - t_i} N_{i,p-1}(t) + \frac{t_{i+p+1} - t}{t_{i+p+1} - t_{i+1}} N_{i+1,p-1}(t) \quad , \quad for\ p > 1. \tag{3.8}$$

When the independent variable is not spatial (e.g., time normalized, as in the current case), the control point coordinates are interpreted as spline coefficients. By using this parameterization, each Cartesian trajectory is represented by 3*m* spline coefficients, where *m* is the number of knots. For the current analysis, nine uniformly spaced knots were used. The spline coefficients were fitted using a least-squares fitting procedure in R software.

Step 2B: Identification of Important Trajectories Using Group Variable Selection

Filtering Stage: Group Nonnegative Garrote (GNNG). Motions described by the spline coefficients of trajectories still have a high dimension when many trajectories are considered as potential predictors. GNNG (Yuan and Lin 2006, Paynabar *et al.* 2014) is a group variable selection method that can reduce data dimensionality by grouping predictors into certain categories and only selecting those that are important for prediction. GNNG is mathematically defined as follows:

$$\min_{d_k} \frac{1}{2}\left\| \mathbf{y} - \sum_{k=1}^{K} \mathbf{X}_k \hat{\beta}_k^{\text{ols}} d_k \right\|^2 + \lambda \sum_{k=1}^{K} d_k, \quad \text{subject to: } d_k \geq 0,\ k = 1,2,...,K, \tag{3.9}$$

where $\mathbf{y}$ is the vector of observed ingress discomfort responses; $\mathbf{X}_k$, the matrix of predictor variables for joint k (i.e., the B-spline coefficients associated with joint k); $\hat{\beta}_k^{\text{ols}}$, the vector of the estimated coefficients using the ordinary least square estimation method corresponding to group k; d_k, the importance of each group; and λ, a tuning parameter. Conceptually, GNNG optimizes the number of groups selected by penalizing the addition of new groups to the model. The performance of the prediction model highly depends on the choice of λ. An optimal value of λ that minimizes the prediction error is found using the *k*-fold cross-validation method (Hastie *et al.* 2009).

For the current analysis, all trajectories associated with a certain joint were considered a group. GNNG is used in this methodology as a filtering method to exclude joints that are not important for prediction rather than choosing the optimal set of joints. GNNG therefore substantially reduces the computational cost of the SGS method.

Wrapping Stage: Stepwise Group Selection (SGS). SGS is the last stage of the dimension reduction step where the critical trajectories for classification are identified. SGS uses the results obtained from GNNG to identify the optimal trajectory combination that will maximize the classification prediction accuracy (i.e., the number of correct predictions divided by the total number of trials).

The SGS method is a modified version of the well-established stepwise regression method (Draper *et al.* 1966, Hocking 1976). In stepwise regression, variables are added to the regression model one at a time based on the *p* value. Similarly, in SGS, groups (B-spline coefficients of the three Cartesian trajectories from a single joint) are added to the classification model one at a time based on the classification prediction accuracy. In this research, the classification model used for choosing groups was the SVM, which is explained in Section 3.2.5. Figure 3-6 shows the pseudo code for this method. The main advantage of SGS over other methods is that it directly uses the classification model prediction accuracy as a criterion to select joints rather than relying on conventional variable selection criteria such as mean square error (MSE), Akaike information criterion, and Mallows's C_p. This ensures that a group will be added to the model only if it increases its prediction accuracy.

```
Read Joints_Input

Initialize SGS = Ø, SGS_Accuracy = Ø, j = 1

While Joints_Input ≠ Ø

        Let n = number of joints in Joints_Input
        Initialize i = 1, k = 1, max_accuracy = 0, accuracy = 0,
                G = Ø, SVM_input = Ø

        For i ≤ n
                SVM_input = Joints_Input(i) + SGS
                Run SVM model with SVM_input
                Accuracy = Calculate SVM model cross-
                validated prediction accuracy
                If accuracy > max_accuracy
                        max_accuracy = accuracy
                        k = i
                End

        i = i + 1

        End

        G = Joint_Input(k)
        Remove G from Joints_Input
        SGS = SGS + G
        SGS_Accuracy(j) = max_accuracy
        j = j + 1

End
```

Figure 3-6. SGS pseudo code

SGS, as is the case with traditional stepwise methods, is a computationally expensive method. The number of iterations required by SGS to obtain a result is $\frac{g\,(g+1)}{2}$, where g is the number of groups. It can be observed that the computation cost of SGS increases rapidly with the number of groups. Therefore, SGS was preceded by a filtering stage.

3.2.5 Step 3: Classification Using Support Vector Machines (SVM)

The focus in the previous steps was to reduce the dimensionality of the data and to choose the variables that will most accurately predict the subjective response in future trials.

In this step, these variables are used to train a classification model using SVM (Cortes and Vapnik 1995). SVM is a supervised learning model for classifying binary data that has gained popularity in the classification community in recent years because it produces accurate classifiers, avoids overfitting data, and is able to separate data that are not linearly separable (Cherkassky and Ma 2004, Pal and Foody 2010, Vapnik 2013).

The main goal of an SVM is to construct an optimal hyperplane that separates two classes of data. An optimal hyperplane maximizes the distance between the classes and the hyperplane, called the *margin* (Figure 3-7). It can be observed that the optimal hyperplane depends on a small number of data points, also called *support vectors*, which define the optimal margin.

In the simplest case where classes are linearly separable, SVM is defined as follows: Given some training D data,

$$\mathcal{D} = \{(x_i, y_i) \mid x_i \in \mathbb{R}^p, y_i \in \{-1, 1\}\}_i^n. \quad (3.10)$$

Find the hyperplane $w \cdot x - b = 0$, which will maximize the margin; thus,

$$\min_{w,b} ||w|| \qquad \text{Subject to } y_i (w \cdot x - b) \geq 1. \quad (3.11)$$

Because cases are not linearly separable in many applications, SVM uses the so-called kernel trick to perform nonlinear classification. The kernel trick uses a kernel function to map the original data into a higher-dimensional space (inner product space), where the data are linearly separable (Boser *et al.* 1992).

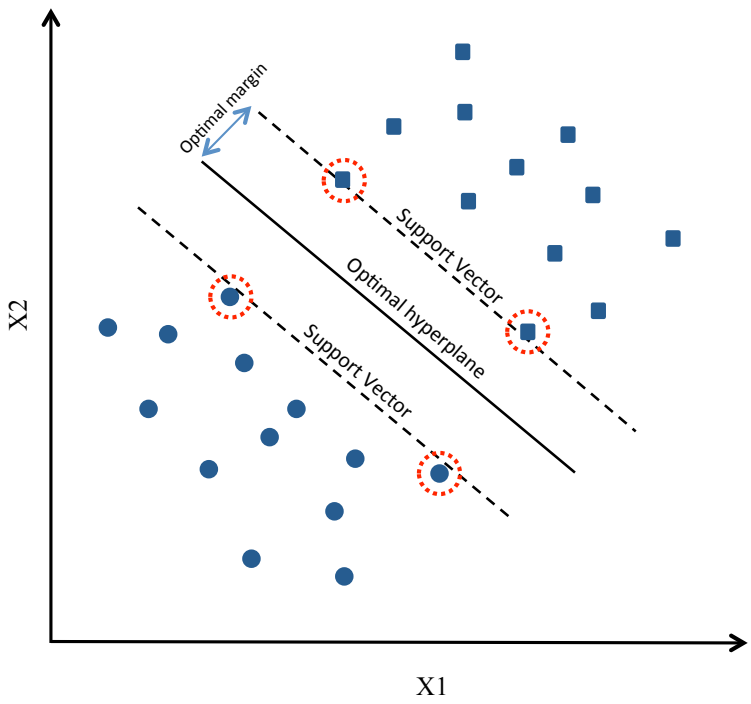

Figure 3-7. SVM illustration—example of a linearly separable case with two variables (adapted from Cortes and Vapnik (1995))

In the current analysis, a Gaussian radial basis function (RBF) kernel was used to train the SVM model. The parameters of the RBF kernel were optimized using grid search to obtain the maximum SVM prediction accuracy (Matheny *et al.* 2007). Moreover, because SVM is a binary classifier, the discomfort response was transformed from a 1 to 10 scale to binary using a range of thresholds (cut points). For example, if a cut point of 5 was used to train the SVM model, responses with a score more than 5 would be labeled as 1 and other responses would be labeled as 0. To assess the performance of an SVM model at a given cut point, the model prediction accuracy was calculated using a 10-fold cross validation.

During the process of developing this framework, many different classification methods in addition to SVM were examined. These include logistic regression, Boosting

(Freund and Schapire 1997), and Random Forests (Breiman 2001). SVM consistently outperformed these methods. However, this observation cannot be generalized to all human motion data without further investigation.

3.3 Results

In this section, the results of applying the proposed framework to the ingress experiment are presented. The results include the selection of B-spline coefficients, the joints selected using GNNG and SGS as well as the prediction accuracy achieved using the final SVM model.

3.3.1 B-spline fitting

At this step the motion trajectories were fit using B-spline fitting. Identifying the number of B-spline coefficients to fit the joint trajectories is an important. Figures 3-8, 3-9, and 3-10 show a comparison between the original curve of the right ankle in the Z-direction and its corresponding reconstructed curve using 8, 9, and 10 B-spline coefficients respectively. We can observe that in Figure 3-8 the reconstructed curve does not represent the original curve nicely, especially at time frames 40-200. Using 9 B-spline coefficients (Figure 3-9), however, gives a much better estimation of the original curve. We can also observe in Figure 3-10 that adding an extra B-spline coefficient did not improve the reconstructed curve. Hence in our analysis we chose 9 bspline coefficients to represent each motion trajectory.

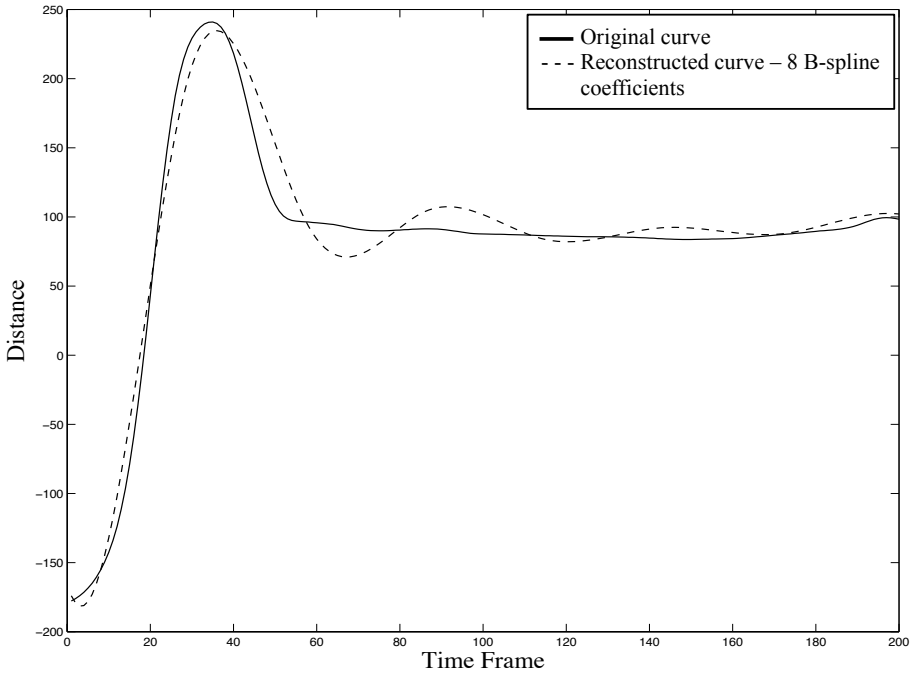

Figure 3-8. Original vs. Reconstructed curves for the right ankle (Z-Direction) using 8 bspline coefficients

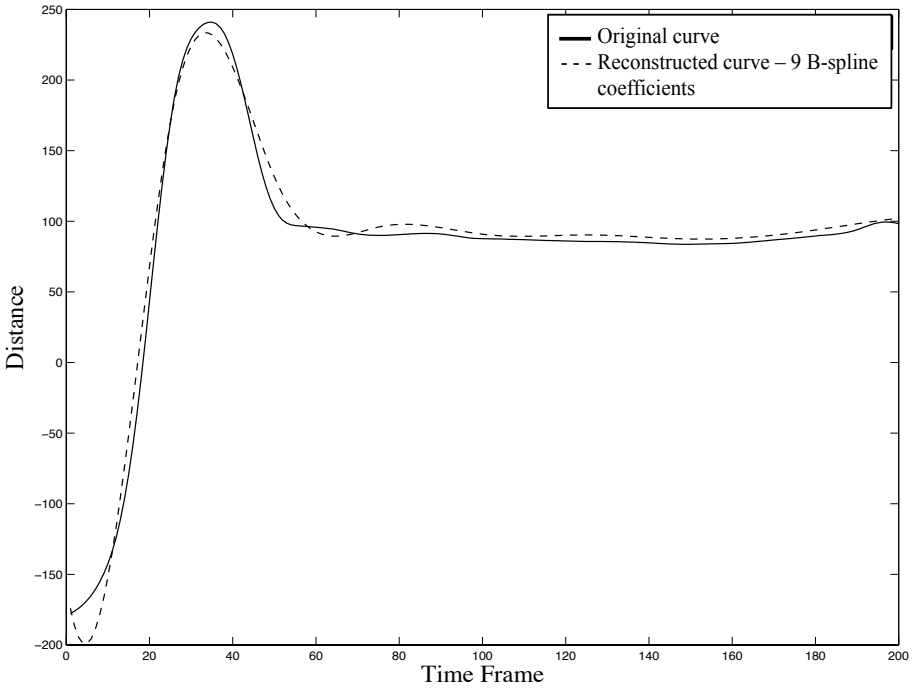

Figure 3-9. Original vs. Reconstructed curves for the right ankle (Z-Direction) using 9 bspline coefficients

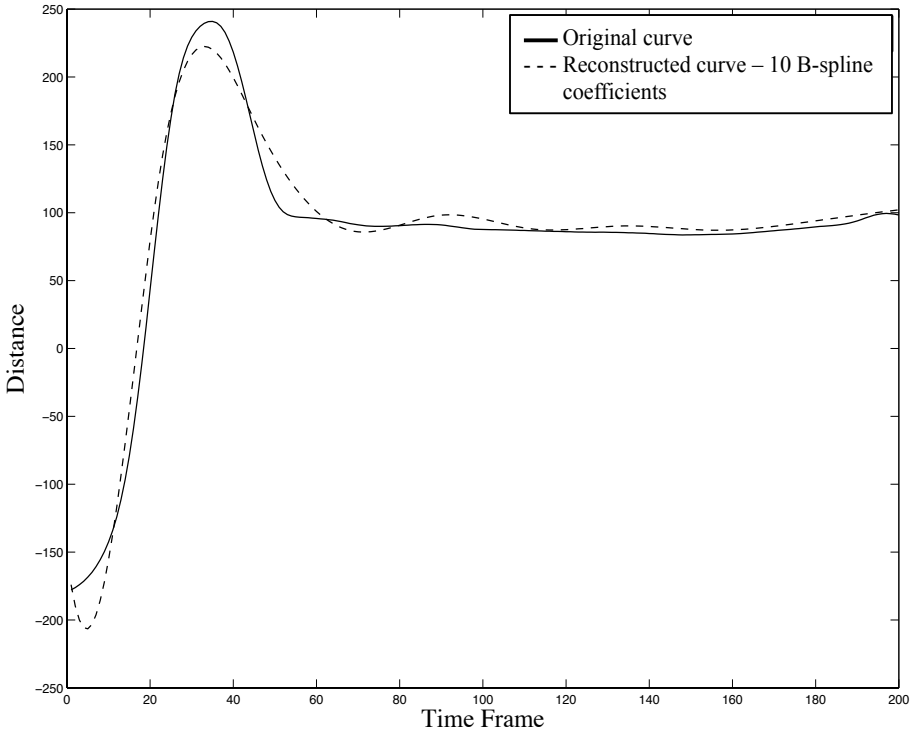

Figure 3-10. Original vs. Reconstructed curves for the right ankle (Z-Direction) using 10 bspline coefficients

3.3.2 Joints Selected

As discussed in Section 3.2.4, trajectories that are important for prediction were identified using a two-stage process: filtering (GNNG) and wrapping (SGS). GNNG was performed on the data set with the discomfort response modeled as a binary response using cut point 5. Using GNNG, 12 of the initial 20 joints were identified as important for prediction. Figure 3-11 shows the results obtained using GNNG. GNNG shrinks the importance factor (d_k) of joints that are not important for prediction to zero; therefore, these joints are not selected. By doing so, GNNG ensures that only the joints that minimize the MSE are selected.

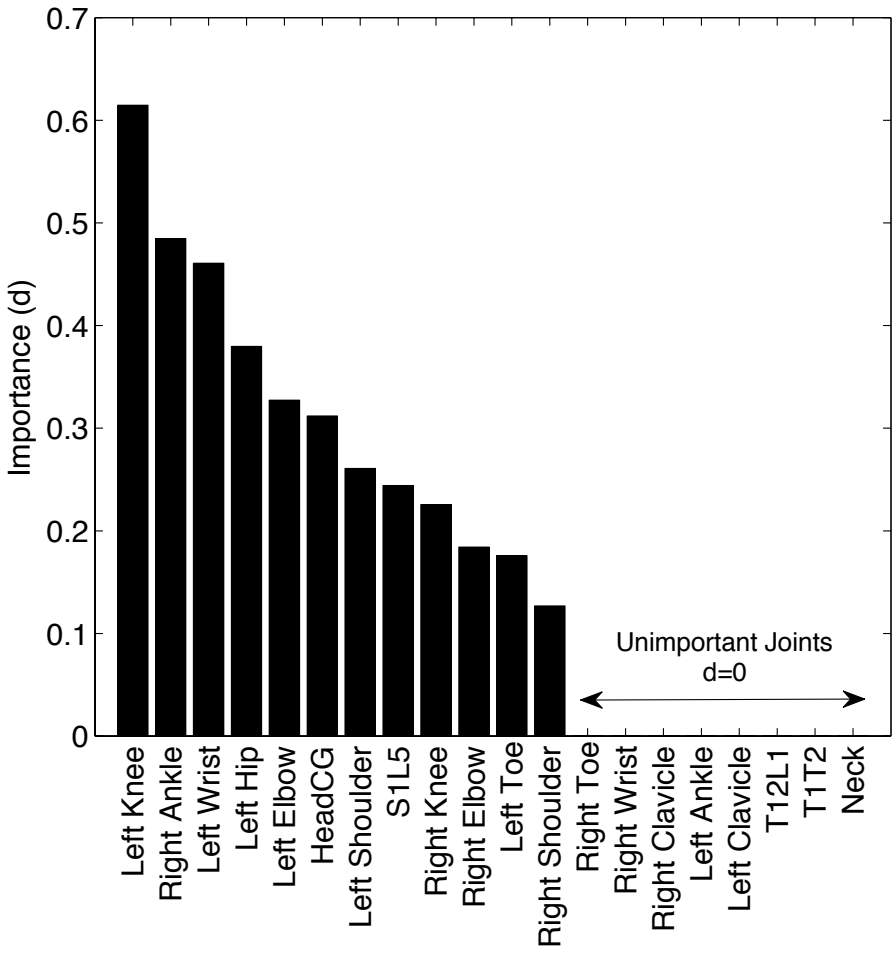

Figure 3-11. Importance of joints using GNNG

The results obtained by GNNG are the main input to SGS. By reducing the number of joints from 20 to 12, GNNG significantly reduces the computational cost of SGS from 210 iterations to 78 iterations, which represents a 63% reduction in the computational cost.

SGS was then performed on these selected joints to choose the optimal set of joints that will maximize the prediction accuracy. Figure 3-12 shows the results of the SGS at each step. The prediction accuracy increases until five joints are added. Subsequently, as more joints are added, the results gradually deteriorate due to overfitting.

The following five joints were finally selected for the SVM model: left hip, right shoulder, right elbow, S1L5, and head. A cut point of 5 was used when performing SGS. Different runs sometimes resulted in different sets of joints. Moreover, using different cut points also resulted in different sets of joints. This occurs because of the high correlation among the joint motions and because SGS uses the prediction accuracy (a random variable) as a criterion to select joints. However, regardless of the specific joint set chosen, the number of joints selected was always 4 or 5, and the prediction accuracy achieved using the selected joints did not vary by more than 1% per specific cut point.

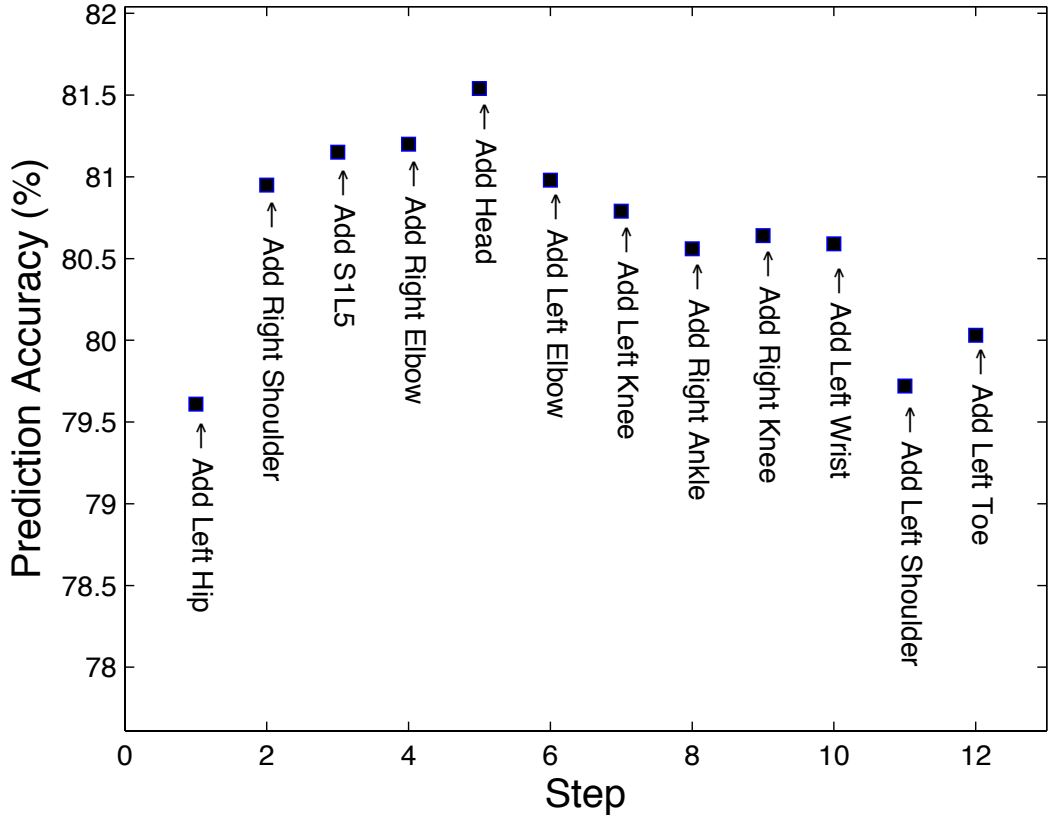

Figure 3-12. SGS results at each step

3.3.3 Prediction Accuracy

SVM models were created for cut points 2 to 7 using the joints selected by SGS. Table 3-1 shows the SVM prediction accuracy using the methodology proposed in this research and the models created using anthropometric and vehicle design variables. The model created using the proposed methodology outperformed the other model at all cut points. Depending on the cut point, the results were improved by between 0.8% and 6.2%. In addition to the improvement in prediction accuracy, the proposed motion-based model is a more robust prediction model than one that is based solely on anthropometric and vehicle design variables. This model can capture important nonlinearities that a simpler model would not. Table 3-1 also shows the prediction accuracy of the model that includes both human motion curves and anthropometric and design variables. The prediction accuracy of these models is very similar to that of the models based on only human motion curves. This confirms our intuition that the trajectory data encode information about the effect of anthropometric and design variables.

Table 3-2 shows the prediction accuracy for the SVM models created using 5 joints (SGS), 12 joints (GNNG), and all 20 joints. Although SGS uses only 5 joints to create the SVM models, it produces models that are on par with and sometimes better than models with a larger number of joints. Future experimenters can therefore use the proposed methodology to track a significantly smaller number of joints without risking the loss of important information.

Table 3-1. Comparison between prediction accuracy using human motion curves and prediction accuracy using anthropometric and design variables

Cut Point	Prediction Accuracy		
	Human motion curves (Using joints selected by SGS)	Anthropometric and design variables	Human motion curves + Anthropometric and design variables
2	83.2	77.0	84.6
3	74.6	73.8	75.3
4	79.6	75.7	79.2
5	81.5	77.6	80.9
6	81.2	79.0	81.2
7	85.5	80.2	86.2

Table 3-2. Prediction accuracy of SVM models using different numbers of joints

Cut Point	Prediction Accuracy		
	SGS (5 joints)	GNNG (12 joints)	All joints (20 joints)
2	83.0	83.8	82.6
3	75.6	75.3	73.6
4	79.8	78.0	76.9
5	81.9	80.0	79.6
6	81.2	80.6	81.3
7	85.5	84.9	84.9

Table 3-3 shows the prediction accuracy results across different vehicle designs. The table also includes sensitivity (i.e. how often does the model predicts 1 when the true rating is 1), specificity (i.e. how often does the model predicts 0 when the true rating is 0), and prevalence (i.e. how often does the rating 1 occur in the dataset). Similarity between the sensitive and specificity rates gives us an indication that the prediction model is not biased towards one class. We can observe from Table 3-3 that the prediction accuracy varies depending on the vehicle design. For example, we can see that vehicle designs 2 and 5 are more difficult to predict than other vehicles. More analysis needs to be done to understand the underlining reason behind that. Furthermore, we can notice that some vehicle designs have similar sensitivity and specificity results, indicating that the model is not biased towards one class, while some designs don't. Non-similarity between sensitivity and specificity results is usually associated with high or low prevalence. For example, design 9 has a low prevalence rate of 23.81% (i.e. only 23.81% of comfort ratings were 1), which is reflected in the sensitivity result. Although the SVM tuning parameters were selected in this study to maximize prediction accuracy, they can be selected to achieve other goals such as maximizing sensitivity or specificity rates.

Table 3-3. Prediction accuracy results for different vehicle designs

Vehicle Design	Prediction Accuracy	Sensitivity	Specificity	Prevalence
1	94.44%	100.00%	94.12%	5.56%
2	61.90%	64.29%	57.14%	66.67%
3	87.50%	100.00%	83.33%	25.00%
4	66.67%	73.33%	50.00%	71.43%
5	58.33%	63.64%	53.85%	45.83%
6	95.24%	0.00%	100.00%	4.76%
7	80.95%	88.89%	33.33%	85.71%
8	100.00%	100.00%	100.00%	5.00%
9	80.95%	20.00%	100.00%	23.81%
10	75.00%	33.33%	92.86%	30.00%
11	85.00%	94.12%	33.33%	85.00%
13	73.91%	66.67%	75.00%	13.04%
14	85.00%	100.00%	50.00%	70.00%
15	76.19%	16.67%	100.00%	28.57%
16	63.16%	76.92%	33.33%	68.42%
17	90.91%	33.33%	100.00%	13.64%
18	90.48%	0.00%	95.00%	4.76%
All vehicles	81.50%	75.55%	84.23%	37.80%

3.4 Discussion

The analysis in this chapter showed that the subjective ratings of ingress difficulty could be better predicted using motion data than solely with information about the vehicle layout and driver body dimensions. This suggests that the use of simulated human motion data to analyze candidate vehicle designs has promise for providing more accurate assessments.

The analysis in this paper only used motion trials that followed the right-leg-first ingress strategy, which was the dominant strategy in this dataset. Analyzing motion trials with other strategies, such as buttock-first strategy, might give different insights and results.

At a broader level, this work is the first to use a functional analysis of motion data to predict a subjective response. Coupled with accurate human motion simulation that takes into account vehicle and anthropometric factors, such as body dimensions and age, this method could have substantial utility, reducing the need for prototype builds and physical testing.

The extension of this methodology to other situations would seem to be limited by the need for detailed motion capture data. However, rapid advances in markerless motion capture using ordinary video cameras (Baker and Kanade 2005, Corazza *et al.* 2006) are reducing the investment needed to obtain good-quality data. Furthermore, the analysis in this chapter shows that, at least for this application, only a relatively sparse set of data is needed to obtain good prediction accuracy. This suggests potential applications in domains in which obtaining even subjective responses would be intrusive.

However, broader applications of this methodology can be anticipated. At a high level, this method extracts features from grouped time series data that provide good predictions of binary covariates. By providing an application-focused method for identifying the ideal sparsity in the input data set, this method can improve the efficiency of building classifiers in many domains.

This study has important limitations based on the nature of the underlying data. In particular, a relatively small number of participants were studied in laboratory conditions. The presence of motion capture markers may have altered the participants' motions, and the range of mockup conditions presented could have influenced the ratings. A study with actual vehicles and a different range of conditions might have produced different results.

The utility of the feature-selection procedures depends considerably on the available data and their relation to the outcome variables. For example, the potential inputs could be largely unrelated to the output, in which case only poor classifiers could be produced. In the current case, most of the variance in the output variable was generated by the experimental manipulation (changing the vehicle geometry over a large range). If all of the data were obtained from a single vehicle, most of the variance would have been due to between-subject variability, and the creation of a good classifier would not be assured.

Additional work is needed to improve our understanding of the relationships between human motion and subjective response, with particular attention to partitioning the sources of variation. Understanding the variations between individuals and the effects of vehicle variables on these sources of variation will help develop better prediction models.

3.5 Conclusion

This chapter presents a framework that enables users to predict subjective responses using human motion curves. Several tools were used to overcome the challenges presented by the complexity of motion curves, including curve registration, curve fitting, group variable selection, and binary classification. The results obtained using this method for predicting ingress discomfort were significantly more accurate than those of a model using anthropometric and design variables as inputs. This framework also enables the use of a small number of joint trajectories to predict discomfort without loss of prediction accuracy.

CHAPTER IV
Sample Size Calculations for a Functional Human Motion Analysis: Application to Vehicle Ingress Comfort Prediction

4.1 Introduction

The ease of getting into a vehicle, known as ingress, is an important consideration for customer satisfaction in the automotive industry (Morgans and Thorness 2013). This has motivated vehicle manufacturers to focus on assessing and improving ingress discomfort. The most straightforward way to assess ingress discomfort is to build prototypes or mockups and have human participants test these potential vehicle designs. Participants rate the ease of getting into the vehicle using a Likert scale. For example, using a 10-point scale, participants might rate a design 1 out of 10 if it is very difficult to get into the vehicle and 10 out of 10 if the ingress motion is exceptionally comfortable. These ingress ratings can also be transformed into binary responses using a cutpoint. Using cutpoint 5, for example, ratings below or equal to 5 are transformed to 0 (or "uncomfortable") and ratings above 5 are transformed to 1 (or "comfortable"). One metric of interest is the proportion of participants who rated the ingress discomfort of a design above a defined cutpoint, referred to as *response proportion* (RP). As the population RP (true RP) for a certain vehicle design is unknown, the participants responses are usually considered as a sample for estimating the population ingress discomfort proportion, which is denoted as $\widetilde{RP}$ in this research.

As it is generally expensive and time-consuming to conduct tests with participants to assess ingress discomfort, manufacturers seek more efficient ways to assess ingress discomfort, including computer simulation (Wegner *et al.* 2007). Advances in digital human modeling technologies have provided the ability to simulate the ingress motion of

people with a wide range of anthropometric features (Reed *et al.* 2006, Reed and Huang 2008). However, even if accurate methods for simulating ingress motions are available, it is still necessary to predict the subjective responses from the motion data. Masoud *et al.* (2014) developed a systematic framework that used human motion trajectories to predict subjective ingress discomfort responses using a machine-learning approach based on support vector machines (SVM). By using this framework, the RP of a vehicle design can be predicted by conducting simulations for a wide range of drivers (e.g., tall and short, young and old) and predicting subjective responses from the simulated motion data. This simulation-based approach can expedite the vehicle design validation process and reduce the cost of testing participants in physical mockups. To differentiate between the estimated RP obtained using participant responses ($\widetilde{\text{RP}}$) and the predicted RP obtained using actual or simulated human motion data, we denote the latter as $\widehat{\text{RP}}$.

In many cases, manufacturers are interested in knowing whether the ingress comfort of one design is better than that of another. For this purpose, manufacturers may conduct a statistical hypothesis test to examine whether the RP of one design is significantly higher than that of another. Moreover, after a design change has been made, manufacturers seek to determine the minimum sample size that can provide a definitive assessment of the difference between two designs in terms of their RP values. In literature, many methods have been developed to test whether there is a significant difference between two proportions (Newcombe 1998). Power calculations and sample size determination for testing the difference between proportions have also been studied (Faul *et al.* 2007, Cohen 2013). In these methods, the responses used to estimate the proportions are assumed to be i.i.d (independent and identically distributed) and to follow

a binomial distribution, i.e., each response has an equal probability of success (p) and the standard deviation of the sample proportions is equal to $\sigma_p = \sqrt{\frac{p\,(1-p)}{n}}$. Although this assumption is appropriate for $\widehat{RP}$, which is estimated using subjective responses, it is not immediately apparent that this relationship can be used to estimate the standard deviation of $\widehat{RP}$ due to the complex relationship between the motion model parameterization and the predicted subjective responses.

The objective of this chapter is to develop a method for conducting power calculations in comparing two $\widehat{RP}$s in which the response proportion $\widehat{RP}$s are predicted from functional data obtained either from physical or virtual experiments. To conduct the power calculations, we must estimate the standard deviation of $\widehat{RP}$, referred to as σ_{RP} in this research. We developed a dual-bootstrapping approach that enables us to consider the two sources of variation in σ_{RP}. One is the modeling variation, which is due to the uncertainty of the estimated prediction model (σ_m) under different training datasets, and the other is the sampling variation due to the randomness of selecting test participants from the population (σ_s).

4.2 Methods

4.2.1 Data Source

The data in this study was obtained from a vehicle ingress experiment that was conducted to study and improve vehicle ingress discomfort (Masoud *et al.* 2014). In brief, the experiment captured human motion data from 32 participants during vehicle ingress trials. Participants evaluated 17 vehicle designs that differed widely in the layout of the driver entry area. During each ingress test, reflective markers were used to record the

location over time (trajectories) of 20 different joints. The trajectories of each joint were modeled by 27 B-spline coefficients. After participants completed an ingress trial (sample), they rated the ease of getting into the car on a 10-point scale, where 1 represents an unacceptable ingress experience and 10, an exceptionally comfortable ingress experience. The ingress discomfort rating was then transformed into a binary response using the cutpoint equal to 5, i.e., ratings below or equal to 5 were set as 0, and those above 5 were set as 1. In research, the Cartesian trajectories of the 5 joints identified by Masoud *et al.* (2014) as the most informative joints for predicting ingress discomfort were used.

4.2.2 Methodology Overview

A dual bootstrap or resampling approach was developed to estimate σ_{RP}, which includes two types of variation, σ_m and σ_s. A bootstrap approach is necessary because the complex relationship between the motion model and the predicted subjective responses precludes the use of the binomial distribution for estimating the standard deviation for the response proportion $\widehat{RP}$. As shown in Figure 4-1, the first step is to generate a set of "bootstrap training datasets" by randomly resampling from the original dataset (X_t, Y_t) obtained from physical participant-tests described in Section 4.2.1, where X_t is the human motion data and Y_t, the corresponding participant ingress discomfort response. Each of the generated bootstrap training datasets (X_t^{*b}, Y_t^{*b}) ($b=1,\ldots, B$) is used to train a prediction model using an SVM classifier (Masoud *et al.* 2014). With B bootstrap training datasets, we can obtain a set of prediction models, i.e., B different SVM classifiers, as shown in Figure 4-1. The second step is to generate "bootstrap prediction

datasets" for the two designs to be compared. As shown in Figure 4-1, the bootstrap prediction datasets are generated by randomly resampling from X_p to generate J bootstrap prediction datasets $X_p^{*1}, X_p^{*2}, \dots, X_p^{*j}, \dots, X_p^{*J}$. These bootstrap prediction datasets are then used along with one trained SVM model to predict J $\widehat{RP}$s for the design of interest (i.e., one $\widehat{RP}$ for each bootstrap prediction dataset). These predicted $\widehat{RP}$s are used to predict the sampling variance (σ_s) that arises due to the randomness in the prediction dataset. By repeating this process B times, through each of the SVM models, we can estimate the modeling variance (σ_m) induced by the uncertainty in the estimated prediction models. The details of each step are discussed in the following subsections.

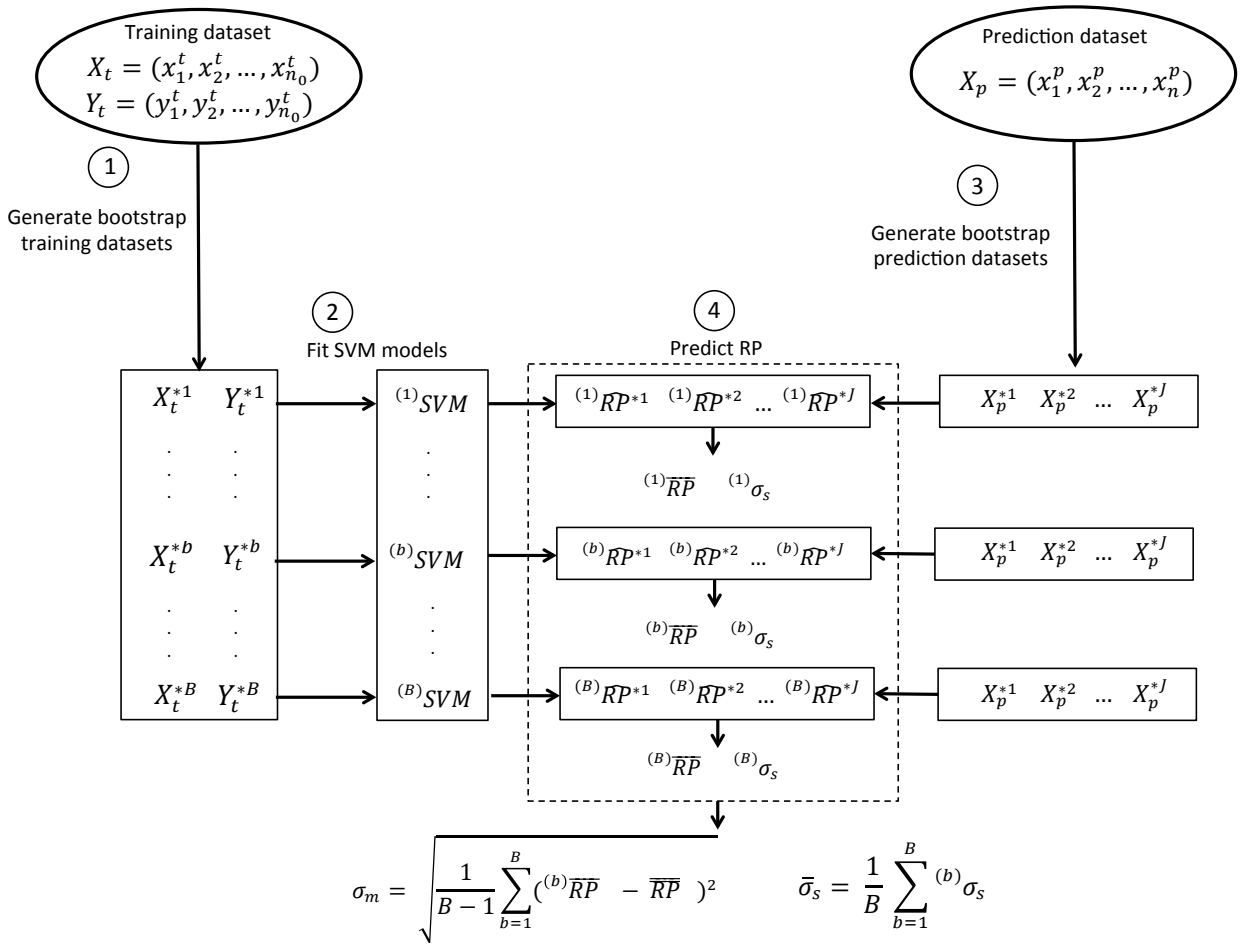

Figure 4-1. Methodology overview

4.2.3 Generate Bootstrap Training Datasets

Assume that $X_t = (x_1^t, x_2^t, \dots, x_{n_0}^t)$ represents the original training dataset obtained from the human participant-tests, where x_i^t represents the vector of human motion data of one ingress sample, represented as B-spline coefficients; n_0, the number of samples; and $Y_t = (y_1^t, y_2^t, \dots, y_{n_0}^t)$, the participant's binary ingress discomfort responses, where y_i^t is the discomfort rating corresponding to the motion data sample x_i^t. A bootstrap training dataset $X_t^{*b} = (x_1^{*b}, x_2^{*b}, \dots, x_{n_0}^{*b})$, $Y_t^{*b} = (y_1^{*b}, y_2^{*b}, \dots, y_{n_0}^{*b})$ is generated by randomly resampling, with replacement, n_0 times from the original dataset X_t and Y_t, where * represents a bootstrap sample and b, the bootstrap replication index. This replication process is performed B times to generate a large number of bootstrap training datasets $X_t^{*1}, X_t^{*2}, \dots, X_t^{*B}$ and $Y_t^{*1}, Y_t^{*2}, \dots, Y_t^{*B}$. In this analysis, the number of bootstrap datasets, denoted as B, was set to 100.

4.2.4 Train SVM Prediction Models

In this step, the bootstrap training datasets are used to train SVM prediction models (Cortes and Vapnik 1995). SVM is a supervised learning classifier that has gained popularity in recent years as it can handle nonlinear classification and is robust to outliers (Cherkassky and Ma 2004, Pal and Foody 2010).

In this work, each set of bootstrap training datasets, X_t^{*b} and Y_t^{*b}, was used to train a separate SVM classifier, thus generating B different SVM models $({}^{(1)}SVM, {}^{(2)}SVM, \dots, {}^{(b)}SVM, \dots, {}^{(B)}SVM)$. The SVM models were trained using a Gaussian RBF kernel. The parameters of the RBF kernel were optimized for the original datasets X_t and Y_t using grid search to minimize the bias between the RP estimated from

the prediction model ($\widehat{RP}$) and that estimated from participant responses ($\widetilde{RP}$); i.e., $\sum_{d=1}^{D}(\widehat{RP}_d - \widetilde{RP}_d)^2$ is minimized, where d is the index of different vehicle designs. Details of training an SVM model for classifying functional data can be found in Masoud et al. (2014).

4.2.5 Generate Bootstrap Prediction Datasets

Assume that $X_p = \left(x_1^p, x_2^p, \ldots, x_n^p\right)$ and $X_{p\prime} = (x_1^{p\prime}, x_2^{p\prime}, \ldots, x_n^{p\prime})$ represent the human motion data corresponding to two different designs indicated by subscripts p and p' respectively, where n represents the number of motion data samples obtained though visual experimental tests or computer simulations. The participants tested in Design p can be either different from those in Design p', referred to as independent datasets, or can be the same, referred to as paired datasets.

At this second bootstrap, bootstrap prediction datasets are generated for each of the two designs by following the same procedure as that used for generating the training datasets. The generated bootstrap prediction datasets for Design p and design p' are denoted as X_p^{*1}, $X_p^{*2}, \ldots, X_p^{*j}, \ldots, X_p^{*J}$ and $X_{p\prime}^{*1}$, $X_{p\prime}^{*2}, \ldots, X_{p\prime}^{*j}, \ldots X_{p\prime}^{*J}$ respectively. Each dataset has sample size equal to n. The number of bootstrap datasets generated was set as J=100

4.2.6 Estimate RP and its Standard Deviation Using Bootstrap Prediction Datasets

In this step, the RP of the design of interest was estimated using the bootstrap prediction datasets. Specifically, a trained SVM model ($^{(b)}SVM$) was used to predict the

ingress discomfort ratings Y_p^{*j} for the datasets X_p^{*j}. Subsequently, one sample of the estimated $\widehat{RP}$ was calculated as

$$\widehat{RP}^{*j} = \frac{1}{n}\sum_{i=1}^{n} y_i^{*j}. \quad (4.1)$$

where y_i^{*j} is the binary ingress discomfort predicted by the b^{th} SVM model for the bootstrap iteration j. Similarly, this process was conducted on all J bootstrap prediction datasets, producing a set of estimates $({}^{(b)}\widehat{RP}^{*1}, {}^{(b)}\widehat{RP}^{*2}, \ldots, {}^{(b)}\widehat{RP}^{*J}.)$ The standard deviation of the sampling variation $({}^{(b)}\sigma_s)$ was then estimated by

$${}^{(b)}\sigma_s = \sqrt{\frac{1}{J-1}\sum_{j=1}^{J}({}^{(b)}\widehat{RP}^{*j} - {}^{(b)}\overline{RP})^2} \quad (4.2)$$

where ${}^{(b)}\overline{RP} = \frac{1}{J}\sum_{j=1}^{J} {}^{(b)}\widehat{RP}^{*j}$. These steps were repeated on all B SVM models, thus producing the results of $({}^{(1)}\overline{RP}, {}^{(b)}\overline{RP}, \ldots, {}^{(B)}\overline{RP})$ and $({}^{(1)}\sigma_s, {}^{(b)}\sigma_s, \ldots, {}^{(B)}\sigma_s)$. The standard deviation of the modeling variation was then calculated by

$$\sigma_m = \sqrt{\frac{1}{B-1}\sum_{b=1}^{B}({}^{(b)}\overline{RP} - \overline{\overline{RP}})^2} \quad (4.3)$$

where $\overline{\overline{RP}} = \frac{1}{B}\sum_{b=1}^{B} {}^{(b)}\overline{RP}$. The average standard deviation of the sampling variance is then obtained by

$$\bar{\sigma}_s = \frac{1}{B}\sum_{b=1}^{B} {}^{(b)}\sigma_s \quad (4.4)$$

Finally, the total standard deviation of the RP for the design of interest (p) was calculated as

$$\sigma_{RP_p} = \sqrt{\sigma_m^2 + \bar{\sigma}_s^2} \quad (4.5)$$

All the steps explained in this section were used to estimate the standard deviation of the second design ($\sigma_{RP_{p'}}$). Moreover, for independent observations where the selected participants in Design p are different from those in design p', the standard deviation of the difference ($\widehat{RP}_p - \widehat{RP}_{p'}$) was calculated as

$$\sigma_{\Delta RP} = \sqrt{\sigma^2_{RP_p} + \sigma^2_{RP_{p'}}} \tag{4.6}$$

In contrast, for paired observations where the same participant was selected under both designs, $\sigma_{\Delta RP}$ was calculated as

$$\sigma_{\Delta RP} = \sqrt{\sigma^2_{RP_p} + \sigma^2_{RP_{p'}} - 2\,cov(\widehat{RP}_p, \widehat{RP}_{p'})} \tag{4.7}$$

where

$$cov\left(\widehat{RP}_p, \widehat{RP}_{p'}\right) = \frac{1}{(B)(J-1)} \sum_{b=1}^{B} \sum_{j=1}^{J} ({}^{(b)}\widehat{RP}_p^{*j} - {}^{(b)}\overline{RP}_p)({}^{(b)}\widehat{RP}_{p'}^{*j} - {}^{(b)}\overline{RP}_{p'}) \tag{4.8}$$

It should be clarified that the covariance between $\widehat{RP}_p$ and $\widehat{RP}_{p'}$ will only be evident if the bootstrap is done simultaneously for the two designs, such that a participant who is chosen in the bootstrap prediction sample X_p^{*b} is also chosen in $X_{p'}^{*b}$.

4.2.7 Estimate σ_{RP_p} Under Different Sample Sizes

The value of σ_{RP_p} is a function of the sample size (n) of the original prediction datasets X_p. To analyze the effect of the sample size on σ_{RP_p}, σ_{RP_p} needs to be estimated under various sample sizes (n^*) for a given design p. The resultant estimates of σ_{RP_p} can then be used to evaluate the testing power for comparing two designs under different sample sizes n^*.

To calculate σ_{RP_p} for a sample size n^*, we used a technique called oversampling (Japkowicz 2000). Assume that $X_p = (x_1^p, x_2^p, \dots, x_n^p)$ represents the human motion data of the design of interest, where *n* represents the number of participants. Assume that we are interested in calculating σ_{RP_p} for a dataset with a different sample size n^*. For this purpose, we generated bootstrap prediction datasets $X_p^{*1}, X_p^{*2}, \dots, X_p^{*J}$ from the dataset X_p, where we oversampled with replacement from X_p such that each bootstrap prediction dataset X_p^{*j} (j=1,…,J) has a new sample size n^*. Once the bootstrap prediction datasets are generated, the estimates of σ_{RP_p} and $\sigma_{\Delta RP}$ can be obtained for this new sample size n^*

4.2.8 Hypothesis Testing and Sample Size Determination

Once ($\sigma_{\Delta RP}$) is obtained, it is possible to test whether there is a significant difference between the RP of the two designs. The hypothesis was formulated as follows:

H_0: ΔRP = 0

H_1: $\Delta RP \neq 0$

where $\Delta RP = RP_1 - RP_2$

To conduct this hypothesis test, a standardized test statistic was defined as

$$z = \frac{\Delta\widehat{RP}}{\sigma_{\Delta RP}} \tag{4.9}$$

where $\Delta\widehat{RP} = \overline{\overline{RP}}_1 - \overline{\overline{RP}}_2$. If a normal distribution is assumed for z, the null hypothesis H_0 is rejected when z is larger than $z_{\alpha/2}$, where α is the pre-specified significance level.

The power to detect a difference of $\delta = \Delta RP = RP_1 - RP_2$ was calculated as Power = $2P(|z| > z_{\alpha/2} \mid \delta)$, which can be rewritten as follows:

$$\text{Power} = 1 - \Phi\left[z\alpha_{/2} - \frac{\delta}{\sigma_{\Delta RP}}\right] + \Phi\left[-z\alpha_{/2} - \frac{\delta}{\sigma_{\Delta RP}}\right] \quad (4.10)$$

where Φ is the cumulative distribution function of the standard normal distribution

4.3 Results

4.3.1 Comparing RP Predictions: $\widehat{\text{RP}}$ vs. $\widetilde{RP}$

In this section, we compared the RP predicted using human motion data ($\widehat{\text{RP}}$) with that predicted using direct participant responses ($\widetilde{RP}$). As previously explained in Section 4.1, these two ($\widehat{\text{RP}}$ and $\widetilde{RP}$) are the estimates of the true (unknown) RP. The closeness between $\widehat{\text{RP}}$ and $\widetilde{RP}$ will give us an indication of how well the prediction model is performing and give us more confidence to use $\widehat{\text{RP}}$ for evaluating future vehicle designs when human participant responses are not available.

Table 4-1 shows the comparison results between the estimates $\widehat{\text{RP}}$ and $\widetilde{RP}$ in which the top-rated 7 out of 17 vehicle designs are selected based on their $\widetilde{RP}$. For each design, the $\widehat{\text{RP}}$ was calculated such that the motion data of that design was treated as the prediction dataset, and the remaining 6 designs were used to train the SVM model. Table 4-1 shows that the predicted $\widehat{\text{RP}}$ agrees well with the estimated $\widetilde{RP}$ (correlation, r = 0.93). The average absolute bias among these 7 designs was equal to 0.04.

Table 4-1. Comparison of $\widehat{\mathbf{RP}}$ and $\widetilde{\boldsymbol{RP}}$ estimates (SVM model trained using the top 7 vehicle designs)

Vehicle Design	$\widehat{\mathrm{RP}}$	$\widetilde{RP}$	Bias
1	0.6667	0.6667	0
2	0.7143	0.7143	0
3	0.5417	0.458	0.0837
4	0.8095	0.8517	-0.0422
5	0.85	0.85	0
6	0.8	0.7	0.1
7	0.7368	0.6842	0.0526

It is worthwhile to note that in the above comparison, the SVM models were trained using 6 vehicle designs that had relatively high $\widetilde{RP}$ values ($\widetilde{RP} > 0.4$). Choosing designs with relatively similar $\widetilde{RP}$ values (i.e., all high or all low RP values) helps reduce the bias between $\widehat{\mathrm{RP}}$ and $\widetilde{RP}$. This is reasonable for design comparison as, in practice, manufacturers often try to choose the best design among a group of good designs. The methodology presented in this work, however, can still be applied if the model was trained using the data of all vehicle designs. Table 4-2 shows a comparison between $\widehat{\mathrm{RP}}$ and $\widetilde{RP}$ for the same 7 vehicle designs; however, the SVM model was trained using all vehicle designs (excluding the predicted vehicle design). We can observe that $\widehat{\mathrm{RP}}$ and $\widetilde{RP}$ are still highly correlated (r = 0.88); however, the average absolute bias (0.076) of the results in Table 4-2 is larger than that (0.04) of the results in Table 4-1.

Table 4-2. Comparison of $\widehat{\mathbf{RP}}$ and $\widetilde{\boldsymbol{RP}}$ estimates (SVM trained using all vehicle designs)

Vehicle Design	$\widehat{\mathrm{RP}}$	$\widetilde{RP}$	bias
1	0.476	0.6667	-0.1907
2	0.6667	0.7143	-0.0476
3	0.4167	0.4583	-0.0416
4	0.8095	0.8571	-0.0476
5	0.80	0.85	-0.05
6	0.60	0.70	-0.1
7	0.7368	0.6842	0.0526

4.3.2 Statistical Testing and Sample Size Calculations of Comparing Two Vehicle Deigns

In this section, we apply the proposed methodology to estimate σ_{RP_p} for 2 of the 7 selected vehicle designs (designs 2 and 4). The motion data of these two designs were used for predicting $\widehat{\mathrm{RP}}$, while the data for the remaining 5 designs were used as training data for training the SVM models. The predicted $\widehat{\mathrm{RP}}$ of the 2 selected designs were 0.6667 and 0.8095, respectively. In this analysis, only the 18 participants who evaluated both designs were included in the prediction dataset. Two analyses were conducted: one, to determine whether these two designs show significantly different RPs and the other, to determine the sample size required for detecting a difference of $\delta = 0.2$ between the two designs with a testing power no less than 70%.

Using the original training data, 100 bootstrap training datasets were generated each with a sample size n_0 = 104. Each bootstrap training dataset was then used to train an SVM prediction model. Bootstrap prediction datasets were then generated for each design. As we use paired observations in this comparison, the bootstrap resampling was

performed for both designs simultaneously such that the covariance structure was appropriately captured. These bootstrap prediction datasets were then used to estimate the modeling and sampling variance for both designs. The standard deviation $\sigma_{\Delta RP}$ was then calculated based on Eq. (4.7) for the paired observations, which yields $\sigma_{\Delta RP} = 0.0966$.

To test whether the RP of the above two designs differs significantly, the critical value, as defined in Eq. (4.9), was calculated as z = 1.48. If $\alpha = 0.05$ is used, we cannot reject H_0. As $z < z_{\alpha/2} = 1.96$, i.e., we cannot conclude that there is a significant difference between the RPs of the above two designs based on the currently available motion data from these 18 participants.

To further answer how many participants would be required to detect a difference of $\delta = 0.2$ between those two designs, we create bootstrap prediction datasets by applying the oversampling strategy for a wide range of sample sizes, based on which $\sigma_{\Delta RP}$ was estimated for each sample size and the testing power was calculated using Eq. (4.10). Figure 4-2 and Figure 4-3 show the effect of increasing the sample size of the prediction datasets from n^*=18 to n^*=300 on $\sigma_{\Delta RP}$ and the testing power. It should be noted that these curves are theoretically smooth; the irregularity results from the underlying data from which the samples are drawn. From Figure 4-2, we can observe that $\sigma_{\Delta RP}$ decreases as we increase the sample size of the prediction datasets. Figure 4-2 also shows that there is slow decrease in $\sigma_{\Delta RP}$ after the sample size increases to n=200. This shows that the modeling variance (σ_m) is not affected by the increase in the sample size of the prediction dataset. Figure 4-3 shows that 180 samples of each design are needed to achieve 70% power in detecting a 0.2 difference in RP.

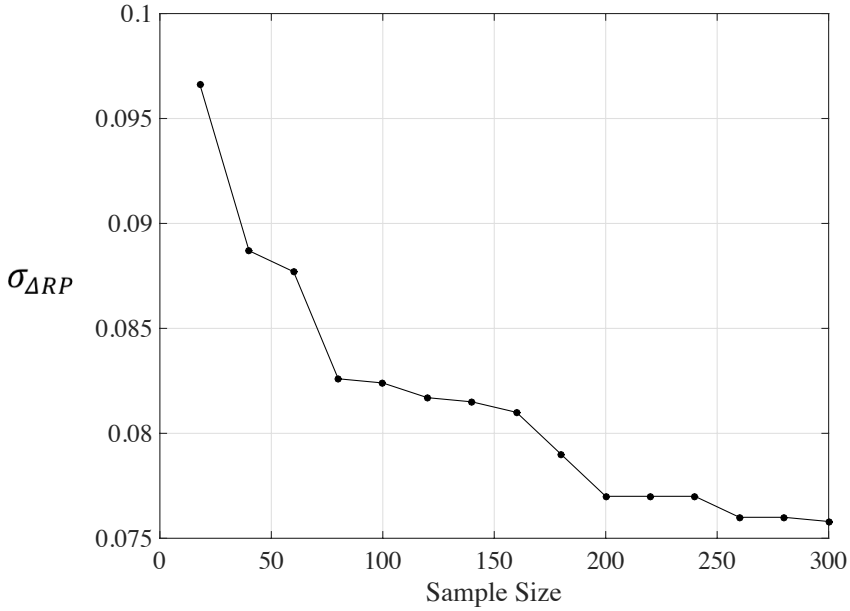

Figure 4-2. Effect of increasing sample size on $\boldsymbol{\sigma_{\Delta RP}}$

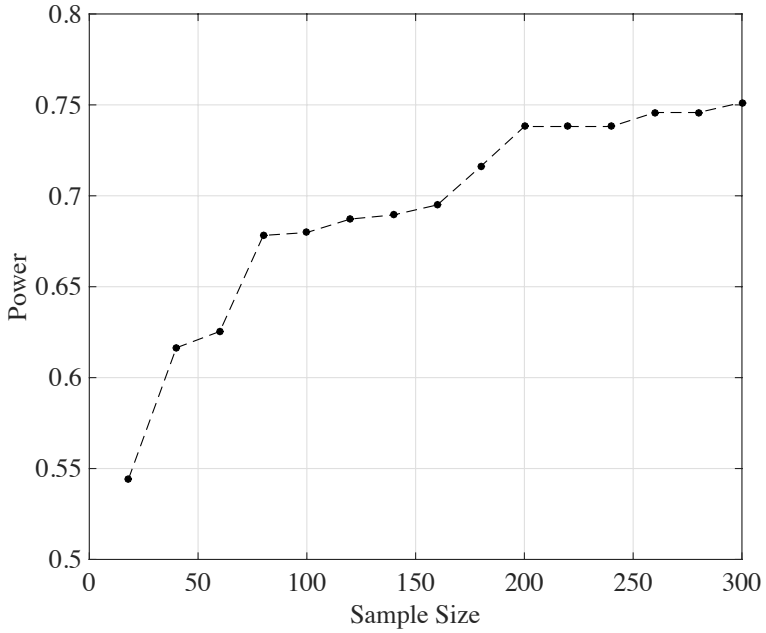

Figure 4-3. Effect of sample size on power to detect a 0.2 difference in RP

4.3.3 Estimating the Sample Size for Different Effect Sizes (δ)

Figure 4-4 illustrates the improvement in power as we increase the sample size of the prediction datasets from n^*=18 to n^*=300 for a range of effect sizes (δ): $\delta = 0.15$, $\delta = 0.20$, and $\delta = 0.25$. We can observe that for effect size $\delta = 0.25$ the number of samples required to achieve a 70% power is 18 samples. We also observe that we cannot achieve a 70% power for $\delta = 0.15$ due to the high modeling variance. Data from more participants would be needed for the training dataset in order to reduce the modeling variance. A similar oversampling technique can be used to estimate the behavior of the modeling variance as we add samples to the training dataset.

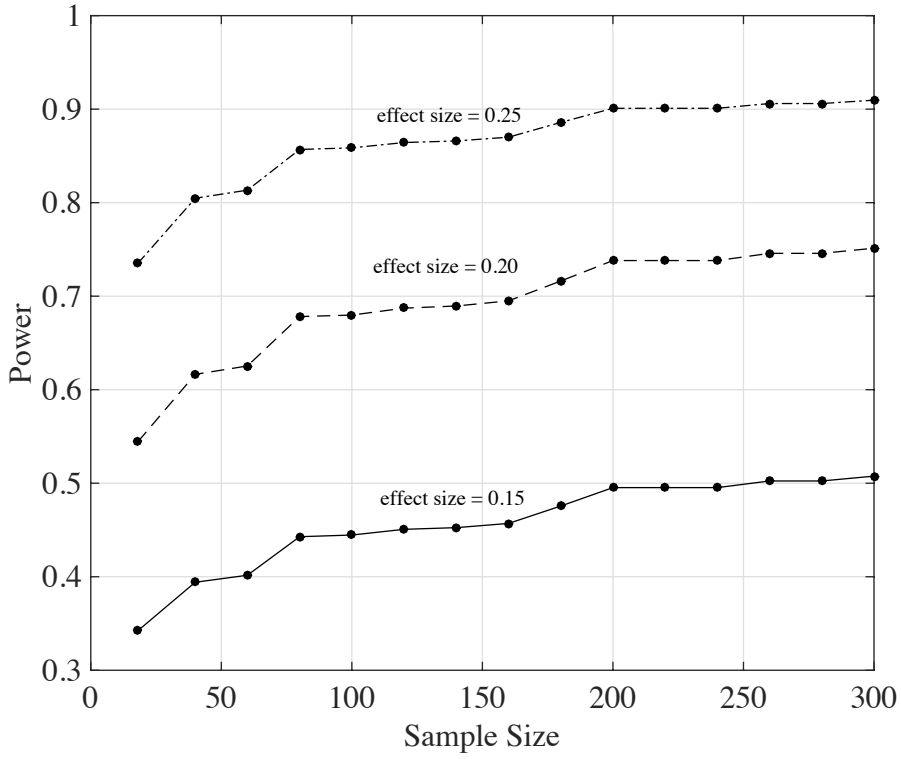

Figure 4-4. Effect of increasing sample size on power for a range of effect sizes.

4.4 Discussion and Conclusion

In this chapter, a new dual bootstrap method was proposed to conduct power calculations for a virtual or physical experimental determination of a binomial outcome based on a functional model. This method was elaborated in the context of estimating the percentage of a driver population who would rate vehicle ingress as "comfortable."

One important contribution is the separate consideration of modeling variance (i.e., the uncertainty of the prediction models) and sampling variance (the uncertainty due to differences in responses among the sampled individuals.) The case study demonstrated that the model variance imposes a bound on the tradeoff between effect size and power. In other words, in some circumstances, a better model may be necessary to achieve a desired power to detect a particular effect size; sampling more individuals for the particular comparison of interest will not help.

The sample size estimated using the methodology presented in this paper represents the upper bound for the samples needed. The methodology assumes that samples are randomly chosen for the population of participants. If the sampling of participants is strategically done such that easy-to-predict participants are sampled less than total number of samples required may be less.

The results for sample size determination shown in the case study are limited by the particular ingress dataset that were used and by the trained SVM prediction models. Different datasets or a different approach to modeling the relationship between the measurable quantities (in this case, motions) and the binary responses to be predicted (in this case, discomfort ratings) might produce different model behaviors. However, the general approach developed here would still be applicable. One essential requirement of

using the proposed method is that the data underlying the prediction model must be available to enable this resampling approach. A different method for estimating model variance would be needed if the original data were not available.

CHAPTER V
Conclusion And Future Research

5.1 Conclusion

The research presented in this dissertation focused on developing new methodologies to facilitate and enable the analysis of human motion data. These methods provide a deeper understanding of the variation in human motion data and enable the prediction of a subjective response based on human motion data as well as statistical testing for proportions estimated using human motion models. First, a UMPCA-based method was developed to analyze human motion variation patterns. Then, a modeling framework was proposed to build a prediction model using human motion data. Moreover, a dual-bootstrap method was developed to enable hypothesis testing and sample size calculation for a proportion estimated using a human motion prediction model. Together, these methods provide useful tools able to facilitate the exploitation of functional data in general and human motion data in particular, and they can help leverage the information contained in such high-dimensional data for more effective decision-making. A detailed summary of the contributions of this dissertation is provided below.

1. *A new UMPCA-based method to analyze the variation patterns of human motion data.* This research introduces a method to analyze the variation patterns of multistream human motion data. This method has the advantage of identifying the important variation patterns of functional data while preserving the original spatiotemporal correlation structure of the data. A simulation study was conducted to demonstrate the superiority of UMPCA over PCA. The study showed that UMPCA was able to capture the important motion patterns more

efficiently than PCA. UMPCA was then applied to a case study based on vehicle ingress, which enabled the motion pattern with the highest variation to be identified. We further verified that this motion pattern is associated with ingress discomfort for these particular test conditions. In addition to the application of this method to vehicle ingress, this method has the potential to be widely applied to many other fields including gait analysis, medical diagnosis, and athletic performance improvement.

2. *A new modeling framework to predict subjective responses using human motion data.* This work introduces a modeling framework capable of predicting subjective discomfort responses using ingress motion curves. This framework addressed the challenges that prevented the previous exploitation of such data, namely, the high dimensionality and misalignment of motion curves. The challenge of high dimensionality was addressed by using B-spline curve fitting and group variable selection methods. In addition, curve registration and normalization methods were proposed to address the misalignment challenge. Finally, an SVM prediction model was built to predict subjective ratings from human motion curves. The analysis presented showed that subjective ratings of ingress difficulty could be better predicted by using motion data rather than by relying solely on information about the vehicle layout and driver's body dimensions. Moreover, the analysis showed that among the 20 joints initially analyzed, five of these contained sufficient information to achieve the maximum prediction accuracy. On a wider level, this research is the first in which the functional analysis of motion data was used to predict a subjective response.

Coupled with accurate human motion simulation that takes into account vehicle and anthropometric factors, such as body dimensions and age, this method could have substantial utility, reducing the need to build a prototype or to perform physical testing.

3. *A new dual-bootstrap method to enable statistical testing on proportions predicted using human motion prediction models.* This research proposes a new dual bootstrap method to conduct power calculations for a virtual or physical experimental determination of a binomial outcome based on a functional model. This method was elaborated in the context of vehicle ingress discomfort assessment where the percentage of the population rating a vehicle as comfortable (RP) was of interest. The dual-bootstrap approach enabled the calculation of the variance of RP, which is a critical element in statistical testing and power calculation. The method also distinguished between the two main sources of variation in the RP: (1) modeling variance due to the uncertainty in the prediction model and (2) sampling variance due to the random sampling of participants from the population. We demonstrated the use of statistical hypothesis tests to determine whether the $\widehat{RP}$ of two vehicle designs are statistically different. We further determined the sample size required to detect an effect δ to achieve a pre-determined power.

5.2 Future Research

As data collection technologies continue to improve, an increasing amount of high-dimension functional data will be available. The analysis of this type of data continues to be a challenge due to its high dimensionality. Yet, due to the usefulness to many fields of

the enormous amount of information contained in this data, researchers continue to be interested in developing new methods to analyze the data. This dissertation introduces methods for facilitating the analysis of functional data, but there is scope for more work in the future. Some possibilities are listed below:

1. In Chapter II, a UMPCA-based method was introduced to identify the important variation patterns in functional data. This method used the hierarchical clustering technique to identify the important joints and time frames for each eigenvector. This step was necessary because the UMPCA method provides eigenvector weights for each joint and time frame even if that weight is practically irrelevant. Therefore, there is a need to develop a Sparse UMPCA method capable of shrinking small eigenvector weights to zero. This is expected to provide more accurate results and easier interpretations for the joint and time frame eigenvectors.
2. In Chapter III, a B-spline basis function was used to fit the human motion curves. The number of knots used in the analysis for each motion curve was nine. The decision regarding the number of knots was based on a visual observation of the quality of the curve fitting over a range of knot numbers. This decision can be subjective as it depends on what an individual believes to be a good fit. This suggests the need for a method that can automatically select the number of b-spline knots required for a given dataset that can achieve the best fit given a predetermined curve-fit quality. This will remove objectivity during the knot selection stage and potentially help provide more informed decisions.

3. In Chapter IV:, the oversampling method was used on the prediction datasets to determine the sample size required to detect an effect δ given a determined power value. This method helped us observe how the sampling variance reduces as we increase the sample size. However, we did not study the possibility of increasing the training sample size to reduce variance due to the model uncertainty. Therefore, there is a need for a method that can be used to study the trade-off between increasing the sample size of the training and the prediction data and determining the most economical choice to achieve the desired goals of the study.
4. Surveillance cameras are one of the largest sources of functional data. Currently, the data collected by surveillance cameras are rarely used to prevent an incident from occurring. Advances in computer vision have enabled the transformation of videos obtained from surveillance cameras to motion curves. A method similar to the framework proposed in Chapter III can be used in conjunction with such curves to predict and prevent an incident from happening. For example, a clothing store can use previous theft incidents to predict that a theft is about to occur based on live data from a surveillance camera. The most demanding research challenge in such an application would be the huge imbalance between the number of safe incidents and the number of theft incidents. Training a classification model with such an imbalanced dataset would be challenging and would require careful consideration.

BIBLIOGRAPHY

Bibliography

Badler, N.I., Allbeck, J., Lee, S-J., Rabbitz, R.J., Broderick, T.T. and Mulkern, K.M. (2005). “New behavioral paradigms for virtual human models.” (No. 2005-01-2689.) SAE Technical Paper.

Baker, S. and T. Kanade (2005). "Shape-from-Silhouette across Time Part Ii: Applications to Human Modeling and Markerless Motion Tracking." International Journal of Computer Vision 63(3), pp. 225-245.

Bellman, R., R. E. Bellman, R. E. Bellman and R. E. Bellman (1961). *Adaptive Control Processes: A Guided Tour*. Princeton University Press, Princeton.

Bharati, M. H., J. J. Liu and J. F. MacGregor (2004). "Image Texture Analysis: Methods and Comparisons." Chemometrics and Intelligent Laboratory Systems 72(1), pp. 57-71.

Boser, B. E., I. M. Guyon and V. N. Vapnik (1992). "A Training Algorithm for Optimal Margin Classifiers." Proceedings of the Fifth Annual Workshop on Computational learning theory, ACM.

Bottoms, D. (1983). "Design Guidelines for Operator Entry-Exit Systems on Mobile Equipment." Applied Ergonomics 14(2), pp. 83-90.

Breiman, L. (2001). "Random Forests." Machine Learning 45(1), pp. 5-32.

Cardot, H., C. Crambes and P. Sarda (2004). "Spline Estimation of Conditional Quantiles for Functional Covariates." Comptes Rendus Mathematique 339(2), pp. 141-144.

Causse, J., X. Wang and L. Denninger (2012). "An Experimental Investigation on the Requirement of Roof Height and Sill Width for Car Ingress and Egress." Ergonomics 55(12), pp. 1596-1611.

Chaffin, D. B. (2007). "Human Motion Simulation for Vehicle and Workplace Design."

Chateauroux, E. (2009). Analysis of the Accessibility Movement to a Car Driver Seat (Focus on the Older Driver Case), PhD Thesis, Ecole Doctorale MEGA de Lyon.

Cherkassky, V. and Y. Ma (2004). "Practical Selection of Svm Parameters and Noise Estimation for Svm Regression." Neural Networks 17(1), pp. 113-126.

Cohen, J. (2013). *Statistical Power Analysis for the Behavioral Sciences*. Academic Press

Cook, R. E., I. Schneider, M. E. Hazlewood, S. J. Hillman and J. E. Robb (2003). "Gait Analysis Alters Decision-Making in Cerebral Palsy." Journal of Pediatric Orthopaedics 23(3), pp. 292-295.

Corazza, S., L. Muendermann, A. Chaudhari, T. Demattio, C. Cobelli and T. P. Andriacchi (2006). "A Markerless Motion Capture System to Study Musculoskeletal Biomechanics: Visual Hull and Simulated Annealing Approach." Annals of Biomedical Engineering 34(6), pp. 1019-1029.

Cortes, C. and V. Vapnik (1995). "Support-Vector Networks." Machine Learning 20(3), pp. 273-297.

Davis, P. J. (1975). Interpolation and Approximation. Courier Corporation.

De Boor, C. (1978). "A Practical Guide to Splines." Mathematics of Computation.

Donoho, D. L. (2000). "High-Dimensional Data Analysis: The Curses and Blessings of Dimensionality." AMS Math Challenges Lecture, pp. 1-32.

Draper, N. R., H. Smith and E. Pownell (1966). Applied Regression Analysis. Wiley New York.

Dufour, F. and X. Wang (2005). Discomfort Assessment of Car Ingress/Egress Motions Using the Concept of Neutral Movement. N. 2005-01-2706, SAE Technical Paper.

Fan, J. and R. Li (2006). "Statistical Challenges with High Dimensionality: Feature Selection in Knowledge Discovery." In Proc. Int. Congr. Mathematicians.

Fan, J. and Y. Fan (2008). "High Dimensional Classification Using Features Annealed Independence Rules." Annals of Statistics 36(6), p. 2605.

Faul, F., E. Erdfelder, A.-G. Lang and A. Buchner (2007). "G* Power 3: A Flexible Statistical Power Analysis Program for the Social, Behavioral, and Biomedical Sciences." Behavior Research Methods 39(2), pp. 175-191.

Freund, Y. and R. E. Schapire (1997). "A Decision-Theoretic Generalization of on-Line Learning and an Application to Boosting." Journal of Computer and System Sciences 55(1), pp. 119-139.

Giacomin, J. and S. Quattrocolo (1997). "An Analysis of Human Comfort When Entering and Exiting the Rear Seat of an Automobile." Applied Ergonomics 28(5), pp. 397-406.

Hastie, T., R. Tibshirani, J. Friedman, T. Hastie, J. Friedman and R. Tibshirani (2009). The Elements of Statistical Learning. Springer, New York, pp. 472-479.

He, X., D. Cai and P. Niyogi (2005). "Tensor Subspace Analysis." Advances in Neural Information Processing Systems.

Hocking, R. R. (1976). "A Biometrics Invited Paper. The Analysis and Selection of Variables in Linear Regression." Biometrics, pp. 1-49.

Jain, A. K., R. P. W. Duin and J. Mao (2000). "Statistical Pattern Recognition: A Review." IEEE Transactions on Pattern Analysis and Machine Intelligence 22(1), pp. 4-37.

Japkowicz, N. (2000). "The Class Imbalance Problem: Significance and Strategies." Proc. of the Int'l Conf. on Artificial Intelligence, Citeseer.

Kay, R. M., S. Dennis, S. Rethlefsen, D. L. Skaggs and V. T. Tolo (2000). "Impact of Postoperative Gait Analysis on Orthopaedic Care." Clinical Orthopaedics and Related Research 374, pp. 259-264.

Kim, S. and K. Lee (2009). "Development of Discomfort Evaluation Method for Car Ingress Motion." International Journal of Automotive Technology 10(5), pp. 619-627.

Knudson, D. V. (2013). Qualitative Diagnosis of Human Movement: Improving Performance in Sport and Exercise. Human Kinetics, pp. 16-38.

Kohavi, R. and G. H. John (1997). "Wrappers for Feature Subset Selection." Artificial intelligence 97(1), pp. 273-324.

Kolda, T. G. and B. W. Bader (2009). "Tensor Decompositions and Applications." SIAM Review 51(3), pp. 455-500.

Li, H., S. Wu, S. Ba, S. Lin and Y. Zhang (2006). Advances in Multimedia Modeling. Springer, New York, pp. 73-82.

Lu, H., K. N. Plataniotis and A. N. Venetsanopoulos (2009). "Uncorrelated Multilinear Discriminant Analysis with Regularization and Aggregation for Tensor Object Recognition." IEEE Transactions on Neural Networks 20(1), pp. 103-123.

Lu, H., K. N. Plataniotis and A. N. Venetsanopoulos (2009). "Uncorrelated Multilinear Principal Component Analysis for Unsupervised Multilinear Subspace Learning." IEEE Transactions on Neural Networks 20(11), pp. 1820-1836.

Mason, C. R., J. E. Gomez and T. J. Ebner (2001). "Hand Synergies During Reach-to-Grasp." Journal of Neurophysiology 86(6), pp. 2896-2910.

Masoud, H. I., M. P. Reed, K. Paynabar, J. J. Jin, K. K. Kozak, N. Wang, J. Wan and G. Gomez-Levi (2014). "Predicting Subjective Responses from Human Motion: Application to Vehicle Ingress Assessment." ASME 2014 International Manufacturing Science and Engineering Conference, American Society of Mechanical Engineers.

Matheny, M. E., F. S. Resnic, N. Arora and L. Ohno-Machado (2007). "Effects of Svm Parameter Optimization on Discrimination and Calibration for Post-Procedural Pci Mortality." Journal of Biomedical Informatics 40(6), pp. 688-697.

Morgans, S. and B. Thorness (2013). *Power: How JD Power III Became the Auto Industry's Adviser, Confessor, and Eyewitness to History*. Greenleaf Book Group.

Newcombe, R. G. (1998). "Interval Estimation for the Difference between Independent Proportions: Comparison of Eleven Methods." Statistics in Medicine 17(8), pp. 873-890.

Pal, M. and G. M. Foody (2010). "Feature Selection for Classification of Hyperspectral Data by Svm." IEEE Transactions on Geoscience and Remote Sensing 48(5), pp. 2297-2307.

Paynabar, K., J. Jin and M. Pacella (2013). "Monitoring and Diagnosis of Multichannel Nonlinear Profile Variations Using Uncorrelated Multilinear Principal Component Analysis." IIE Transactions 45(11), pp. 1235-1247.

Paynabar, K., J. Jin and M. P. Reed (2014). "Informative Sensor and Feature Selection Via Hierarchical Non-Negative Garrote." Technometrics (just accepted).

Petzäll, J. (1995). "The Design of Entrances of Taxis for Elderly and Disabled Passengers: An Experimental Study." Applied Ergonomics 26(5), pp. 343-352.

Ramsay, J. and X. Li (1998). "Curve Registration." Journal of the Royal Statistical Society: Series B (Statistical Methodology) 60(2), pp. 351-363.

Reed, M. P., J. Faraway, D. B. Chaffin and B. J. Martin (2006). The Humosim Ergonomics Framework: A New Approach to Digital Human Simulation for Ergonomic Analysis, SAE Technical Paper.

Reed, M. P. and S. Huang (2008). Modeling Vehicle Ingress and Egress Using the Human Motion Simulation Framework. N. 2008-01-1896, SAE Technical Paper.

Silverman, B. and J. Ramsay (2005). Functional Data Analysis. Springer.

Simon, S. R. (2004). "Quantification of Human Motion: Gait Analysis—Benefits and Limitations to Its Application to Clinical Problems." Journal of Biomechanics 37(12), pp. 1869-1880.

Vapnik, V. (1998). *Statistical Learning Theory*. Wiley New York.

Vapnik, V. (2013). The Nature of Statistical Learning Theory. Springer Science & Business Media.

Wang, L., W. Hu and T. Tan (2003). "Recent Developments in Human Motion Analysis." Pattern Recognition 36(3), pp. 585-601.

Wegner, D., J. Chiang, B. Kemmer, D. Lämkull and R. Roll (2007). Digital Human Modeling Requirements and Standardization. N. 2007-01-2498, SAE International Conference of Digital Human Modeling.

Yan, H., K. Paynabar and J. Shi (2015). "Image-Based Process Monitoring Using Low-Rank Tensor Decomposition."

Yuan, M. and Y. Lin (2006). "Model Selection and Estimation in Regression with Grouped Variables." Journal of the Royal Statistical Society: Series B (Statistical Methodology) 68(1), pp. 49-67.